Available online at www.sciencedirect.com

ScienceDirect

Geochimica et Cosmochimica Acta 144 (2014) 126–156

Geochimica et Cosmochimica Acta

www.elsevier.com/locate/gca

Aragonite, breunnerite, calcite and dolomite in the CM carbonaceous chondrites: High fidelity recorders of progressive parent body aqueous alteration

Martin R. Lee, Paula Lindgren *, Mahmood R. Sofe

School of Geographical and Earth Sciences, University of Glasgow, Glasgow G12 8QQ, UK

Received 16 May 2014; accepted in revised form 17 August 2014; available online 29 August 2014

Abstract

Carbonate minerals in CM carbonaceous chondrite meteorites, along with the silicates and sulphides with which they are intergrown, provide a detailed record of the nature and evolution of parent body porosity and permeability, and the chemical composition, temperature and longevity of aqueous solutions. Fourteen meteorites were studied that range in petrologic subtype from mildly aqueously altered CM2.5 to completely hydrated CM2.0. All of them contain calcite, whereas aragonite occurs only in the CM2.5–CM2.2 meteorites and dolomite in the CM2.2–CM2.0. All of the aragonite crystals, and most of the calcite and dolomite grains, formed during early stages of parent body aqueous alteration by cementation of pores produced by the melting of tens of micrometre size particles of H_2O-rich ice. Aragonite was the first carbonate to precipitate in the CM2.5 to CM2.2 meteorites, and grew from magnesium-rich solutions. In the least altered of these meteorites the aragonite crystals formed in clusters owing to physical restriction of aqueous fluids within the low permeability matrix. The strong correlation between the petrologic subtype of a meteorite, the abundance of its aragonite crystals and the proportion of them that have preserved crystal faces, is because aragonite was dissolved in the more altered meteorites on account of their higher permeability, and/or greater longevity of the aqueous solutions. Dolomite and breunnerite formed instead of aragonite in some of the CM2.1 and CM2.2 meteorites owing to higher parent body temperatures. The pore spaces that remained after precipitation of aragonite, dolomite and breunnerite cements were occluded by calcite. Following completion of cementation, the carbonates were partially replaced by phyllosilicates and sulphides. Calcite in the CM2.5–CM2.2 meteorites was replaced by Fe-rich serpentine and tochilinite, followed by Mg-rich serpentine. In the CM2.1 and CM2.0 meteorites dolomite, breunnerite and calcite were replaced by Fe-rich serpentine and Fe–Ni sulphide, again followed by Mg-rich serpentine. The difference between meteorites in the mineralogy of their replacive sulphides may again reflect greater temperatures in the parent body regions from where the more highly altered CMs were derived. This transition from Fe-rich to Mg-rich carbonate replacement products mirrors the chemical evolution of parent body solutions in response to consumption of Fe-rich primary minerals followed by the more resistant Mg-rich anhydrous silicates. Almost all of the CMs examined contain a second generation of calcite that formed after the sulphides and phyllosilicates and by replacement of remaining anhydrous silicates and dolomite (dedolomitization). The Ca and CO_2 required for this replacive calcite is likely to have been sourced by dissolution of earlier formed carbonates, and ions may have been transported over metre-plus distances through high permeability conduits that were created by impact fracturing.

* Corresponding author.
E-mail address: paula.lindgren@glasgow.ac.uk (P. Lindgren).

http://dx.doi.org/10.1016/j.gca.2014.08.019
0016-7037/

1. INTRODUCTION

The CM carbonaceous chondrites were altered from their original anhydrous mineralogy by aqueous fluids shortly after parent body accretion (e.g., DuFresne and Anders, 1962; McSween, 1979; Bunch and Chang, 1980). Differences between meteorites in the abundance and chemical composition of phyllosilicates relative to their original constituents (i.e., silicate, metal and amorphous materials) is the principle measure of the extent of their alteration (e.g., McSween, 1979; Browning et al., 1996; Zolensky et al., 1997; Rubin et al., 2007; Howard et al., 2009, 2011). Assuming that all of the CMs had a comparable initial mineralogy, inter-meteorite differences in their degree of alteration reflect contrasts in one or more of: (i) temperature; (ii) water/rock ratio; (iii) duration of aqueous activity. Despite being the volumetrically dominant alteration products, phyllosilicates in the meteorite matrix and chondrule rims are difficult to use for exploring the relative importance of these three variables because they are very finely crystalline and intergrown with other alteration products and original anhydrous minerals (e.g., Barber, 1981; Tomeoka and Buseck, 1985). The disequilibrium nature of this assemblage has led some to speculate that a proportion of the minerals that are assumed to be the products of *in situ* alteration were instead sourced from a precursor body or formed within the solar nebula (Bunch and Chang, 1980; Metzler et al., 1992; Ciesla et al., 2003; Howard et al., 2011). However, the fine-scale admixture of anhydrous and hydrous minerals more likely just reflects mineral-controlled alteration within a rock matrix of very low porosity and permeability (Bland et al., 2009; Velbel et al., 2012).

Serpentine that has partially replaced olivine and clinopyroxene in some of the less highly altered CMs have been used successfully to probe the aqueous environment. Hanowski and Brearley (2001) and Velbel et al. (2012, 2013) showed that this serpentine is uniform in composition throughout ALH 81002, Nogoya and QUE 93005, respectively, despite the wide range in chemistry of the anhydrous silicates that it had replaced. Thus the chemistry of serpentine was determined by the composition of the solution, not the reactant, and the aqueous fluids that mediated serpentinisation were chemically homogenous at least on the length scale of an individual meteorite (i.e., ~1 to 10 cm). Homogenisation of solution chemistry by diffusion was enabled by pervasive but static fluids, and/or long alteration timescales (Velbel et al., 2012).

Carbonates are a minor component of most CMs, typically attaining a few percent by volume. Although it has been suggested that they formed prior to accretion of the final parent body (Metzler et al., 1992), and even in the atmospheres of stars (Kemper et al., 2002), the commonplace compositional zoning of CM carbonates (e.g., Brearley, 1998, 2006a) and their occasional occurrence within veins (Lindgren et al., 2011, 2012; Lee et al., 2013a) is consistent with precipitation from liquid water. Application of the $^{53}Mn/^{53}Cr$ chronometer has shown that the carbonates formed soon after parent body accretion (e.g., Brearley and Hutcheon, 2000, 2002; de Leuw et al., 2009; Lee et al., 2012), and Fujiya et al. (2012) have recently found that calcite and dolomite in different CMs formed synchronously at 4563 + 0.4/−0.5 Ma. These minerals have several properties that potentially make them powerful tools for analysing alteration conditions: (i) their solubility means that carbonates may respond to the evolving parent body environment by one or more of dissolution, recrystallization or replacement; (ii) they can indicate paths of fluid movement via their petrographic context (e.g. by the presence of veins); (iii) their chemical compositions record solution chemistry and Eh (redox potential); (iv) compositional differences between grains of any one carbonate generation can be used to explore spatial variations in solution properties, whereas compositional differences within grains (i.e., zoning) provide information on temporal fluctuations in fluid chemistry; (v) their oxygen isotope values reflect both the temperatures of aqueous solutions and the extent to which they have reacted with anhydrous silicates ($\delta^{18}O$ and $\Delta^{17}O$ both fall with progressive water/rock interaction; Clayton and Mayeda, 1999; Benedix et al., 2003). Differences in the chemical and isotopic compositions of carbonates between meteorites with contrasting degrees of alteration confirms that these minerals have the potential to provide a high fidelity record of environmental conditions (Johnson and Prinz, 1993; Riciputi et al., 1994; Benedix et al., 2003; de Leuw et al., 2010). For example, dolomite has been described only from the more highly altered CMs (Johnson and Prinz, 1993; Riciputi et al., 1994), and calcite in these meteorites also has a narrower range of Fe concentrations than in the less highly altered CMs (de Leuw et al., 2010). Benedix et al. (2003) demonstrated a good correspondence between the degree of alteration of a suite of CMs, the petrographic properties of their calcite grains, and bulk carbonate $\delta^{18}O$ and $\Delta^{17}O$ values.

The aims of the present study are understand better the origin, movement and chemical evolution of parent body aqueous solutions by examining the mineralogy, microstructure and petrographic context of carbonates along with the silicate and sulphide minerals with which they are intergrown. We have examined 14 CMs that span a wide range of degrees of aqueous alteration, and integrated our findings with results from previous studies (Supplementary Table 1). Specifically, in the framework of a progressive alteration sequence (Rubin et al., 2007), we have sought to describe, quantify and account for: (i) intra- and inter-meteorite differences in the properties of carbonates, including their mineralogy, abundance, grain size and degree of replacement by phyllosilicates and sulphides, and (ii) mechanisms of crystal growth, focusing on evidence for cementation versus replacement. This information will help answer the key question in CM carbonaceous chondrite evolution, including whether greater degrees of aqueous processing correlate with one or more of higher water/rock ratios, temperatures or the longevity of parent body fluids.

2. SAMPLES AND METHODOLOGY

The 14 CM carbonaceous chondrites studied span a wide range of degrees of preterrestrial aqueous alteration, and include falls and Antarctic finds (Table 1). The degree

Table 1
The meteorites examined in this study.

Meteorite	Date and location	Total mass (g)	Weathering (W) and fracturing (F) grades
ALH 83001[a]	Find (1983, Antarctica)	3019	W = Be
ALH 88045 (P11448)[b,g]	Find (1988, Antarctica)	18	n/a
Cold Bokkeveld (1964, 705)[a,g]	Fall (1838, South Africa)	5200	n/a
EET 96029,9[c]	Find (1996, Antarctica)	843.3	W = A/B
LAP 031166,15[d]	Find (2003, Antarctica)	15.1	W = B; F = B
LON 94101,15[a]	Find (1994, Antarctica)	2804.6	W = Be
MET 01070,17[e]	Find (2001, Antarctica)	40.6	W = Be
Mighei (P7253)[a,g]	Fall (1889, Ukraine)	8000	n/a
Murchison (P11449)[a,g]	Fall (1969, Australia)	~4500	n/a
Murray (BM1966, 48)[a,g]	Fall (1950, USA)	1260	n/a
Nogoya (P84191)[a,g]	Fall (1879, Argentina)	4000	n/a
Pollen (P7249)[l,g]	Fall (1942, Norway)	254	n/a
QUE 93005,10[a]	Find (1993, Antarctica)	13.4	W = A/Be
SCO 06043,10[f]	Find (2006, Antarctica)	27.6	W = B/CE

Antarctic meteorite abbreviations: ALH, Allan Hills; EET, Elephant Moraine; LAP, LaPaz Ice Field; LON, Lonewolf Nunataks; MET, Meteorite Hills; QUE, Queen Alexandra Range; SCO, Scott Glaciers.
n/a denotes not applicable.
[a] Information from the Meteoritical Bulletin Database.
[b] Wlotzka (1990).
[c] Grossman (1998).
[d] Connolly et al. (2007).
[e] Russell et al. (2003).
[f] Weisberg et al. (2008).
[g] Loaned by the Natural History Museum (London).

of aqueous alteration of each of these meteorites is described using the petrologic subtype scheme of Rubin et al. (2007), whereby CM2.5 denotes the least altered meteorite in our suite and CM2.0 is the most highly aqueously processed (Table 2). Those meteorites whose petrologic subtype has yet to be determined are referred to as "CM2.x". Table 2 also lists the degree of alteration of some members of the sample suite with reference to the mineral alteration index (MAI) of Browning et al. (1996), and the ratio of anhydrous Fe, Mg silicates to phyllosilicates (Howard et al., 2009, 2011).

2.1. SEM imaging, X-ray microanalysis and EBSD

Carbonate grains were located in carbon coated thin sections by backscattered electron (BSE) imaging and

Table 2
The 14 meteorites examined in this study listed by their degree of aqueous alteration.

Meteorite	Subtype	MAI[d]	Phyllosilicate/anhydrous[e]
EET 96029	CM2.5[a]	———	———
Murchison	CM2.5[b]	0.43	3.10
Murray	CM2.4/2.5[b]	0.57	3.24
Pollen	CM2.4[a]	0.53	———
Mighei	CM2.3[a]	0.77	3.74
LON 94101	CM2.2–2.3[a]	———	———
Nogoya	CM2.2[a,f]	0.97	4.09
Cold Bokkeveld	CM2.2[b]	1.03	4.87
ALH 83001	CM2.1[c]	———	9.23
LAP 031166	CM2.1[a]	———	———
QUE 93005	CM2.1[b]	———	6.54
ALH 88045	CM2.0[a]	———	———
MET 01070	CM2.0[b]	———	11.40–11.48
SCO 06043	CM2.0[a]	———	13.85

———, not determined.
[a] Petrologic subtype determined in the present study using the criteria of Rubin et al. (2007).
[b] Classified by Rubin et al. (2007).
[c] Classified by de Leuw et al. (2010).
[d] Mineral Alteration Index of Browning et al. (1996).
[e] Determined by Howard et al. (2009, 2011) using X-ray diffraction.
[f] The Nogoya thin section contains two lithologies, a CM2.2 and the other more like a CM2.3.

energy-dispersive X-ray (EDX) microanalysis. This work used two field-emission SEMs, both operated at 20 kV: a FEI Quanta 200F equipped with an EDAX silicon-drift EDX detector operated through a Genesis system and a Zeiss Sigma equipped with an Oxford Instruments X-Max silicon-drift EDX detector operated through an AZTEC system. The abundance of carbonate minerals was determined by point counting using the SEM; typically 500–1000 points were counted per thin section with a 290 μm step between points. Grain sizes were measured from BSE images with the longest dimension quoted; unless stated otherwise the sizes of 25 grains of each carbonate type were measured for each sample. Pores within carbonate grains were characterized using BSE and SE (secondary electron) images. Microporous carbonate refers to regions in carbonate grains were the dominant sizes of pores are >100 nm, and nanoporous carbonate refers to regions were the dominant sizes of the pores are much smaller than 100 nm, although some can reach 200 nm. SEM-CL (cathodoluminescence) images were obtained using a KE Developments panchromatic CL detector attached to the Quanta SEM. Following the procedures of Lee et al. (2005), the images were acquired at a very slow scan speed in order to overcome the deleterious effects of phosphorescence.

Electron backscatter diffraction (EBSD) was used to distinguish aragonite from calcite, and to determine the crystallographic orientations of both minerals. After polishing for ~30 s. in colloidal silica, uncoated thin sections were mapped using an EDAX-TSL system attached to the Quanta SEM. The microscope was operated at 20 kV and in low vacuum (~50 Pa) mode; the beam current was relatively high, but is not quantified by this instrument. In each scan the Kikuchi patterns were indexed by allowing the TSL OIM 5.2 software to choose between structure files for aragonite (Pmcn: $a = 0.496$ nm, $b = 0.797$ nm, $c = 0.574$ nm) and calcite ($R\bar{3}c$: $a = 0.4991$ nm, $c = 1.7062$ nm, $\beta = 120°$). The EBSD data are expressed as maps and pole figures. Image quality (IQ) maps represent the quality of Kikuchi patterns in greyscale, whereas inverse pole figure (IPF) maps display crystallographic orientations via a colour scale; typically the IPF maps are overlain on IQ maps. The upper hemisphere stereographic pole figures show the orientations of the poles (i.e., normals) to certain lattice planes of single aragonite and calcite crystals.

2.2. Quantitative X-ray microanalysis

Quantitative chemical analyses of carbonates and phyllosilicates were obtained by electron probe microanalysis (EPMA) using a five spectrometer Cameca SX100 electron probe at the University of Edinburgh. For aragonite and calcite the instrument was operated using a 5 mm defocused spot and at 15kV/3 nA to analyse for Na and Ca, and 15 kV/20 nA for Mg, Mn, Fe and Sr. The following standards were used for calibration of mineral compositions: jadeite (Na), spinel (Mg), calcite (Ca), Mn metal (Mn), fayalite (Fe) and celestite (Sr). Typical detection limits (in wt%) were Na (0.04), Mg (0.01), Ca (0.18), Mn (0.05), Fe and Sr (0.04). Those analyses with anomalously high concentrations of Mg and/or Fe (i.e., beyond the maximum values recorded in CM carbonates by de Leuw et al. (2010) of 1.5 mol% $MgCO_3$ and 2.5 mol% $FeCO_3$) were assumed to have been contaminated by rim or matrix phyllosilicates and so were removed from the datasets. In most analyses Mn is below detection limits (i.e., <~0.05 wt%), although as previous EPMA studies have found measurable Mn (de Leuw et al., 2010) it is possible that the standard used may not have been ideal for calibrating carbonates. Analytical results are summarised within the text, with full datasets listed in Supplementary Table 2.

For phyllosilicate analyses the EPMA was operated at 15 kV/10 nA and using a 5 μm defocused spot to measure Na, Al, Mg, Si, Ca, S, Fe and 15 kV/80 nA for P, K, Ti, Cr, Mn, Ni, Sr. The following standards were used for calibration of mineral compositions: jadeite (Na), spinel (Al, Mg), wollastonite (Si, Ca), apatite (P), pyrite (S), orthoclase (K), rutile (Ti), Cr metal (Cr), Mn metal (Mn), fayalite (Fe), Ni metal (Ni), celestine (Sr). Typical detection limits (in wt%) were: Na (0.02), Al (0.03) Mg (0.02), Si (0.05), P (0.01), S (0.03), K (0.01), Ca (0.03), Ti (0.01), Cr (0.02), Mn (0.03), Fe (0.11), Ni (0.02), and Sr (0.03). For calculating the molecular proportions of ions in the Mg-rich serpentine grains, no correction has been made for the potential presence of intergrown Fe–Ni sulphides as was undertaken by Velbel et al. (2012) in their study of Nogoya serpentine. This is because the Mg-rich serpentine grains typically have much lower concentrations of sulphur than the serpentine studied by Velbel et al. (2012) (i.e., typically <0.5 wt.% SO_2 versus 4–8 wt% SO_2, respectively). Analytical results are summarised within the text, with full datasets listed in Supplementary Table 3.

2.3. Raman spectroscopy

Raman spectroscopy used a Renishaw inVia Raman microscope operated with a 514 nm laser that has a spot size of ~1 μm. Laser focusing on the sample was performed through a petrographic microscope equipped with a 100× objective. The spectra were accumulated in 30 increments with a measuring time of 2 s each, using 10% of the total laser power of 50 mW to avoid sample damage. Calibration was made with respect to wave number using a silicon standard. The collected Raman spectra were processed (curve fitted to determine the peak positions) using the Reinshaw WIRE software. Aragonite and calcite were identified using the positions of some of their minor Raman bands; calcite has bands at ~282 and 713 cm^{-1} and aragonite has minor bands at ~207 and 704 cm^{-1} (White, 2009).

2.4. Mineral identification

Dolomite and breunnerite were identified by EDX, whereas Raman spectroscopy and EBSD were used to distinguish aragonite from calcite. As it was impractical to analyse all Ca-carbonate grains in each CM to determine their polymorphs, work focused on those grains with a habit and petrographic context consistent with previously described CM aragonite (Lee and Ellen, 2008). Thus, aragonite abundances quoted are likely to be minimum values.

Many calcite grains have rims and/or inclusions that may be composed of Fe-rich serpentine (e.g., cronstedtite), tochilinite, or a fine-scale intergrowth of the two minerals. These three rim components can be readily distinguished using TEM by their chemical compositions and/or d-spacings. Cronstedtite, $Fe_2^{2+}Fe^{3+}(SiFe^{3+})O_5(OH)_4$, has a ~0.71 nm basal layer spacing whereas Fe-rich tochilinite, $6Fe_{0.9}S$ 5(Fe, Mg)$(OH)_2$, has a ~1.08 nm basal layer spacing. Coherent interstratification of serpentine with tochilinite produces a structure with a ~1.80 nm layer spacing (Mackinnon and Zolensky, 1984). Where TEM data were unavailable, the rims and inclusions are described as tochilinite if Si was undetectable by EDX, or 'serpentine/tochilinite' if Si was present (in addition to O, Mg, S, Fe and Ni). With regards to anhydrous sulphides, CMs can contain troilite (FeS), pyrrhotite ($Fe_{1-x}S$), pentlandite $(Fe-Ni)_9S_8$, and 'intermediate sulphides' with an atomic Ni/(Fe + Ni) ratio of 0.10–0.40 (Rubin et al., 2007). These authors found that pentlandite occurs in CMs of all petrologic subtypes, whereas pyrrhotite is most common in the CM2.6–CM2.3 meteorites, and intermediate sulphides in the CM2.4 to CM.2.0. Where the sulphides have not been quantitatively chemically analysed, they are here described as either 'Fe-sulphide' (i.e., troilite/pyrrhotite) or 'Fe–Ni sulphide' (i.e., pentlandite/intermediate sulphides).

3. RESULTS

Carbonates have been described and classified according to their mineralogy, microstructure, petrographic context, presence of carbonate and non-carbonate inclusions, and the continuity and mineralogy of their rims (Supplementary Fig. 1). As the chemical compositions of CM carbonates have been the topic of several previous studies (i.e., Johnson and Prinz, 1993; Riciputi et al., 1994; de Leuw et al., 2010), our work on carbonate chemistry has concentrated on quantifying compositional differences between aragonite and calcite where they occur together in the same meteorite. Aragonite forms euhedral, subhedral or anhedral crystals. Calcite and dolomite may occur as single crystals, or as polycrystalline grains; the grains are referred to as 'equant' if approximately equidimensional in shape, or otherwise 'irregular'. Calcite and dolomite may also occupy veins. For the description of calcite we have adopted the 'type 1' and 'type 2' terminology that was used by Tyra et al. (2007, 2012) for calcite in EET 96006-paired (CM2.2–2.3). Each of these two types are here further subdivided into two varieties. Type 1a calcite typically occurs as subhedral or anhedral crystals, or equant grains, that are typically less than ~70 μm in size and usually (but not always) have serpentine/tochilinite rims. They are often twinned, may be zoned in CL, and can contain bands of nanopores. Type 1b calcite is similar in most respects to type 1a but lacks serpentine/tochilinite rims and nanopores, and is instead intergrown with coarse Fe-sulphide or Fe–Ni sulphide crystals. Type 2 calcite differs from types 1a and 1b in being finely polycrystalline and microporous, and lacking serpentine/tochilinite rims. Type 2a grains characteristically contain few micrometre size Fe–Ni sulphide inclusions, whereas type 2b calcite is free of sulphides. Where the two varieties of types 1 or 2 calcite are described collectively they are referred to as 'type 1' or 'type 2'. Calcite also occurs in the CM2.1 and CM2.0 meteorites intergrown with breunnerite or dolomite to make 'bimineralic grains', or intergrown with breunnerite and dolomite to make 'polymineralic grains'.

3.1. Aragonite

Aragonite has been has described previously from Cold Bokkeveld, Cochabamba and Murchison (Müller et al., 1979; Barber, 1981; Supplementary Table 1), and in the present study has been found in all meteorites of petrologic subtype CM2.5 to CM2.2 apart for EET 96029 (Fig. 1). It ranges in abundance from 3.20 to 0.03 crystals mm^{-2}, and aragonite is less common in the more highly altered meteorites (Fig. 2; Supplementary Table 4). Murchison, Murray and Pollen aragonite crystals are concentrated in clusters up to 2 mm across, whereas they are uniformly distributed throughout the matrices of Mighei and Cold Bokkeveld. In LON 94101 aragonite crystals are scarce in the vicinity of a millimetre-size calcite vein but otherwise homogeneously dispersed through the sample (Lee et al., 2013a). Nogoya contains two lithologies, a dominant CM2.2 that has no aragonite, and a subordinate lithology that is more like a CM2.3 in its degree of alteration and contains 3 crystals of aragonite.

Aragonite crystals range in size from 5 to 101 μm, and they are slightly coarser in the more highly altered meteorites (Fig. 2; Supplementary Table 4). They may be euhedral or subhedral (i.e., the crystals have at least one straight edge that is parallel to (100), (010) or {110} and so likely to be a crystal face) or anhedral (i.e., all crystal edges are irregular and embayed by the matrix or micropores) (Fig. 3). Euhedral crystals occur only in Murchison and Murray. The proportion of crystals that are euhedral or subhedral falls with increasing degree of aqueous alteration of the host rock (Fig. 2c). Aragonite crystals lack the phyllosilicate and sulphide rims that characterise CM calcite, although they may be cross-cut by fractures (Fig. 3d), and sometimes they contain phyllosilicates. Murchison and Pollen both have aragonite crystals that occur as inclusions within grains of type 1a calcite (Fig. 3e), and Mighei aragonite crystals display SEM-CL zoning (Fig. 3b). The chemical composition of aragonite is summarised in Table 3, and shows that crystals have low concentrations of Mg and Sr, and 0.47–1.61 mol% $FeCO_3$.

3.2. Type 1a calcite

Type 1a calcite occurs in all meteorites of petrologic subtypes CM2.5 to CM2.2 (Fig. 1), and in each it is far more abundant than both aragonite and type 2 calcite. Thus, the volume of Ca-carbonate in the CM2.5–CM2.2 meteorites (Table 4) essentially equals the abundance of type 1a calcite. Ca-carbonate is unusually scarce in EET 96029 and Nogoya, but otherwise ranges from 1.4 to 2.3 vol.%, and its abundance does not correlate with petrologic subtype (Table 4). Type 1a calcite is distributed uniformly through the matrices of all meteorites apart for LON 94101 where it is depleted in the vicinity of a calcite vein (Lee et al., 2013a).

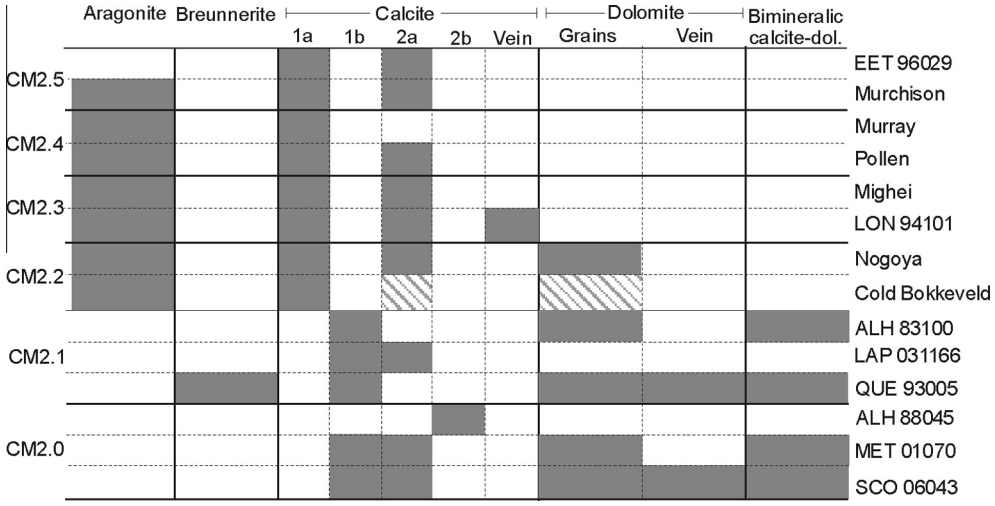

Fig. 1. Summary of the mineralogy and petrographic types of carbonates in the 14 CMs studied. The carbonate types that occur in each meteorite are indicated by a grey box. Type 2a calcite and dolomite were described from Cold Bokkeveld by Johnson and Prinz (1993) and de Leuw et al. (2010), as indicated by the striped boxes.

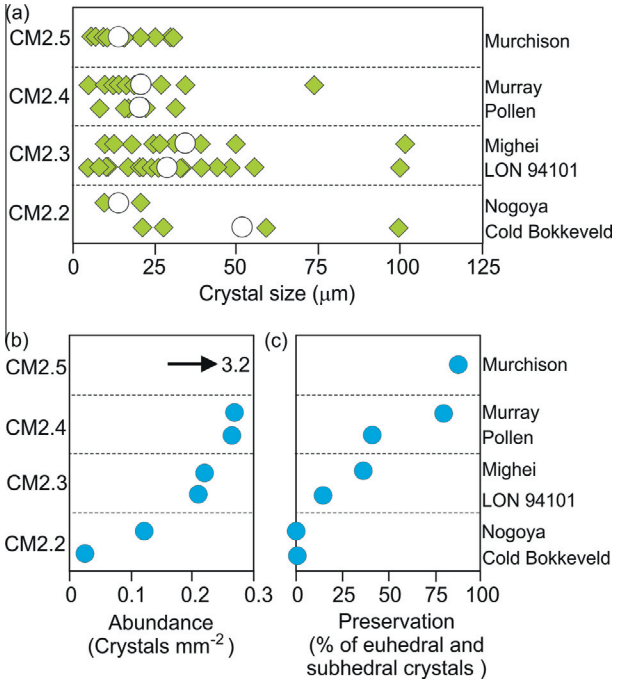

Fig. 2. Plots showing the differences between CMs in the properties of aragonite crystals. (a) Sizes of all of the crystals found. White circles are the average for each meteorite. (b) Abundances of aragonite. The value for Murchison (3.2 crystals mm^{-2}) is not shown. (c) Degree of preservation expressed as the proportion of crystals in each meteorite that are euhedral and subhedral. Values for Murray and LON 94101 are from Lee and Ellen (2008) and Lee et al. (2013a), respectively. The data are listed in Supplementary Table 4.

The calcite occurs as anhedral and subhedral crystals, and irregular and equant grains. The only systematic difference between meteorites is the proportion of subhedral crystals, which are particularly common in Murchison, Murray and Mighei. These crystals have one or more straight edges that are in contact with serpentine/tochilinite, or less frequently the matrix, and an irregular edge that is always in contact with the matrix (Fig. 5a–c). The straight edges lie parallel to the traces of $\{10\bar{1}4\}$, or $\{1\bar{1}00\}$, and so are interpreted to be crystal faces (Fig. 5a–c). Oscillatory zoning of calcite, as revealed by SEM-CL, is commonplace in crystals from Murchison, Murray and Mighei, and also occurs in Pollen and Nogoya calcite (Fig. 5c and d). Zone boundaries are crystallographically controlled (Fig. 5c), and the pattern of zoning shows that any one crystal has formed by growth from one or more nucleation sites (Fig. 5c and d). Some of the subhedral crystals are overgrown by a later generation of type 1a calcite that has a different habit and/or crystallographic orientation (Fig. 6a–d). Type 1a calcite crystals in all meteorites have *e*-twins that may occur in one, or less commonly two orientations (Fig. 6e), and are occasionally curved owing to deformation of their host crystal (Fig. 6b and c).

Type 1a calcite is free of inclusions of the meteorite matrix, but may contain micropores, and micropore-rich grains are especially abundant in EET 96029, Nogoya and Cold Bokkeveld. Straight and narrow micropores have developed along *e*-twin composition planes, whereas irregular micropores occur between the constituents of polycrystalline grains (Fig. 6f). Calcite crystals in Murchison, Murray and Mighei frequently contain bands of pores that lie parallel to zone boundaries and crystal faces (Fig. 7a). Although they can reach 200 nm in size, most are smaller than 100 nm and so the term 'nanopore' is used. Some of these nanopores have crystallographically controlled shapes (Fig. 7b and c) whereas others are irregular (Fig. 7d). The nanoporous calcite has a greater defect density than nanopore-free calcite, and *e*-twins are continuous between the two (Fig. 7d).

Type 1a grains in EET 96029 rims have rims up to 10 μm in thickness that are composed of 5–7 μm long by 1 μm wide tabular crystals that project into the calcite (Fig. 8a).

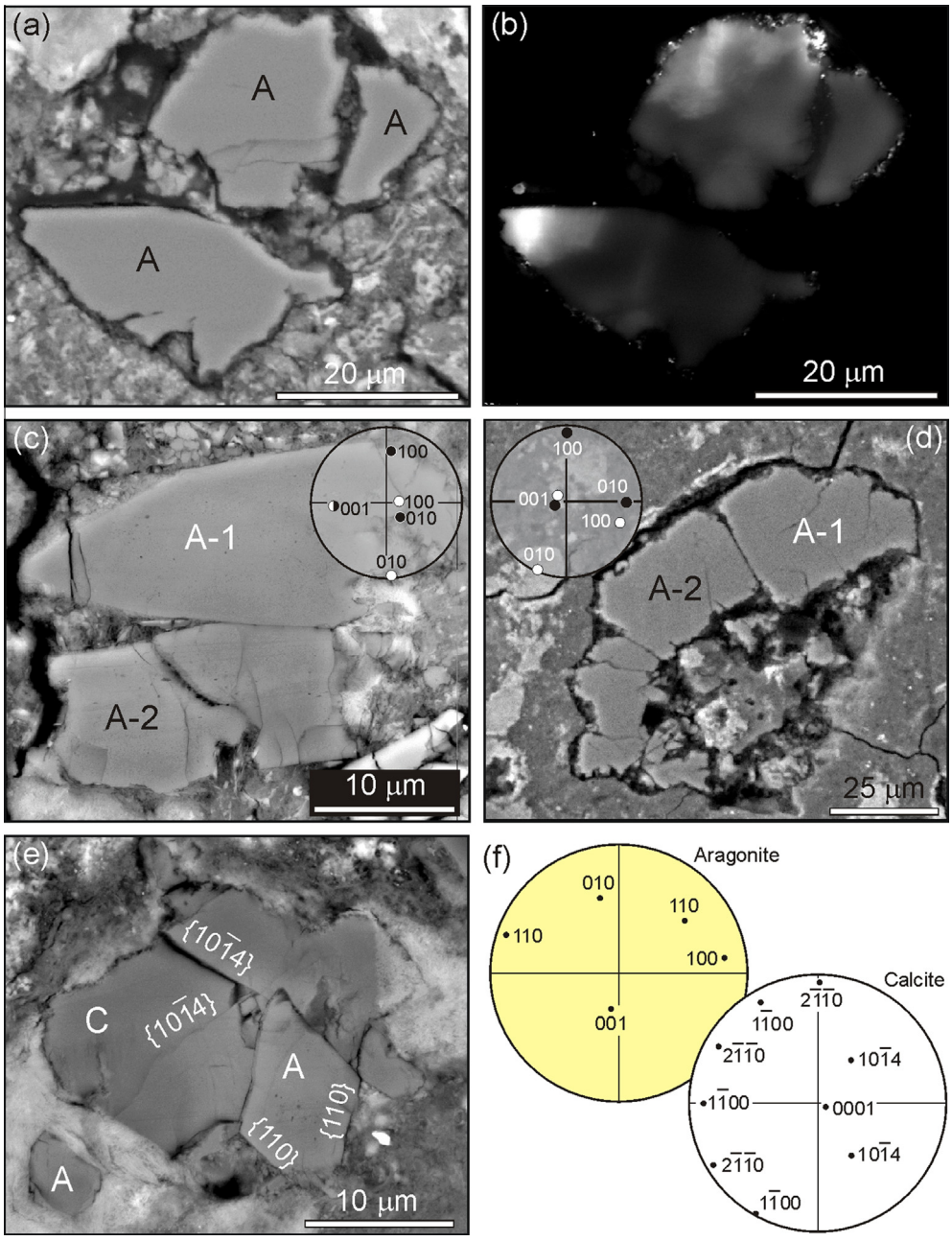

Fig. 3. Crystals of aragonite (A) in meteorite matrices. (a) BSE and (b) SEM-CL images of a pair of aragonite crystals Mighei, one subhedral and the other anhedral. The pattern of zoning shows that the crystals have grown from the left to right. (c) A pair of subhedral aragonite crystals in Murchison. The inset EBSD pole figure shows the orientations of planes in crystal A-1 (white circles) and A-2 (black circles). The two crystals are related by ~80° of rotation about a common *c* axis, i.e., the pole to (001). (d) BSE image of an aragonite grain in Cold Bokkeveld that contains two crystals, whose orientations are shown by the inset EBSD pole figure (crystal A-1 in white circles, A-2 in black circles). The crystals are related by ~100° rotation about their nearly coincident *c* axis. (e) BSE image of a bimineralic aragonite-calcite grain in Murchison. The larger of the crystals of aragonite is subhedral and overgrown by an anhedral crystal of type 1a calcite (C). The calcite crystal has broken along two of its {10$\bar{1}$4} cleavages (labelled) and is partially enclosed by serpentine-tochilinite (white). (f) EBSD pole figures of the subhedral aragonite crystal in (e) and its calcite overgrowth. Both carbonate minerals are oriented with their *c* axis at a high angle to the plane of the thin section, and the aragonite crystal has a {110} habit. Calcite {2$\bar{1}\bar{1}$0} planes are near-parallel to the (010) and {110} planes of aragonite.

Qualitative EDX shows that these rim crystals are composed principally of O, S and Fe. Serpentine/tochilinite forms rims to type 1a calcite grains in all other meteorites (Figs. 6e and 8b–d), although each of these meteorites also contains grains whose calcite is in contact with the matrix (e.g., Fig. 7a), or separated from the matrix by micropores (Fig. 6f). Serpentine/tochilinite rims in Pollen are encrusted by tochilinite fibres (Fig. 8c–e), and rims are especially thick in proportion to the size of their host grains in LON 94101 (Lee et al., 2013a) and Cold Bokkeveld (Fig. 6e). Grains of

Table 3
The chemical composition of aragonite and calcite in those meteorites containing both carbonates.

Meteorite	Mean composition (mol%)						Molar Mg/Ca	
	Ca	Mg	Mn	Fe	Sr	*n*	Carbonate	Solution
Aragonite								
Murchison	98.48	0.28	dl	1.20	0.04	3	0.0028	2.187–2.843
Murray[a]	98.02	0.37	dl	1.61	dl	4	0.0038	2.904–3.775
Mighei	98.96	0.03	dl	0.95	0.06	15	0.0003	0.208–0.270
LON 94101[a]	99.03	0.13	dl	0.77	0.07	12	0.0013	0.990–1.287
Nogoya	99.26	0.12	dl	0.47	0.14	1	0.0012	0.930–1.209
Cold Bokkeveld	98.92	0.12	dl	0.89	0.08	4	0.0012	0.934–1.214
Type 1a calcite								
Murchison	99.08	0.08	0.03	0.81	dl	10	0.0008	0.020–0.080
Murray	98.36	0.10	0.03	1.52	dl	24	0.0010	0.026–0.103
Mighei	98.39	0.19	0.08	1.35	dl	31	0.0019	0.048–0.192
LON 94101[a]	99.32	0.01	dl	0.67	dl	10	0.0001	0.003–0.012
Nogoya	98.94	0.26	0.00	0.81	dl	16	0.0027	0.068–0.274
Cold Bokkeveld	99.05	0.05	dl	0.90	dl	13	0.0005	0.014–0.055

Data obtained by EPMA. Analyses of aragonite uncontaminated by matrix were unobtainable from Pollen. dl denotes below detection limits and *n* denotes number of analyses. All analyses are listed in Supplementary Table 2.

[a] Data for LON 94101 aragonite and calcite from Lee et al. (2013a), and Murray aragonite from Lee and Ellen (2008). Solution compositions were calculated using partition coefficients for Mg into aragonite and calcite of 0.0010–0.0013 and 0.01–0.04, respectively (Huang and Fairchild, 2001; Gaetani and Cohen, 2006).

Table 4
The abundance and grain size of calcite and dolomite.

Meteorite	Abundance (vol.%)		Crystal/grain size (μm)	
	Ca-carbonate[a]	Dolomite	Type 1a calcite range (mean)	Dolomite[c] range (mean)
EET 96029	<0.09	————	26–96 (43)	n/a
Murchison	1.4	————	10–153 (39)	n/a
Murray	1.9	————	18–73 (38)	n/a
Pollen	2.3	————	19–125 (42)	n/a
Mighei	1.5	————	7–43 (24)	n/a
LON 94101	2.3	————	9–51 (26)	n/a
Nogoya	0.4	0.01	14–72 (23)	30–41 (36)
Cold Bokkeveld	1.8	————	10–91 (30)	n/a
ALH 83001	1.5	2.3	15–106 (34)	16–101 (44)
LAP 031166	0.8	————	10–153 (40)	n/a
QUE 93005	2.1	1.8	25–140 (62)	13–97 (46)
ALH 88045	1.1	————	n/a	n/a
MET 01070[b]	2.1	0.4	6–45 (23)	58–110 (92)
SCO 06043	0.6	0.9	17–152 (40)	13–205 (80)

———— denotes absent. n/a denotes not applicable owing to the absence of type 1a calcite or dolomite.

[a] As type 1 calcite is much more abundant than aragonite and type 2 calcite in all meteorites, these values essentially equal the volume of type 1 calcite.

[b] Outside the sulphide lens only. 25 grains measured in all meteorites apart for SCO 06043 ($n = 16$).

[c] Using measurements of the following number of grains: Nogoya (2), ALH 83100 (25), QUE 93005 (25), MET 01070 (4), SCO 06043 (10).

type 1a calcite in all meteorites may contain patches of very finely crystalline Mg-rich serpentine, and these patches are largest in Pollen and Nogoya. Pollen shows a complete range from serpentine/tochilinite rimmed grains of calcite that contain small patches of Mg-rich phyllosilicate (Fig. 8c) to objects that are rimmed by serpentine/tochilinite but are composed solely of Mg-rich serpentine (Fig. 8e). The Mg-rich serpentine in Pollen has Mg/(Mg + Fe) values of 0.67–0.83 (Supplementary Table 3), and data are plotted in Fig. 9. TEM imaging shows that the Mg-rich serpentine crystals are ribbon-shaped and <200 nm long by ~10 nm wide (Fig. 8f). The Mg-rich serpentine has inclusions of serpentine-tochilinite that have started to 'delaminate' at their edges and become incorporated into the Mg-rich serpentine (Fig. 8f).

3.3. Type 1b calcite

Type 1b calcite is present in all of the meteorites of petrologic subtypes CM2.1 and CM2.0 apart for ALH 88045 (Fig. 1), and is far more abundant that type 2 calcite where the two carbonate types occur together. There are no

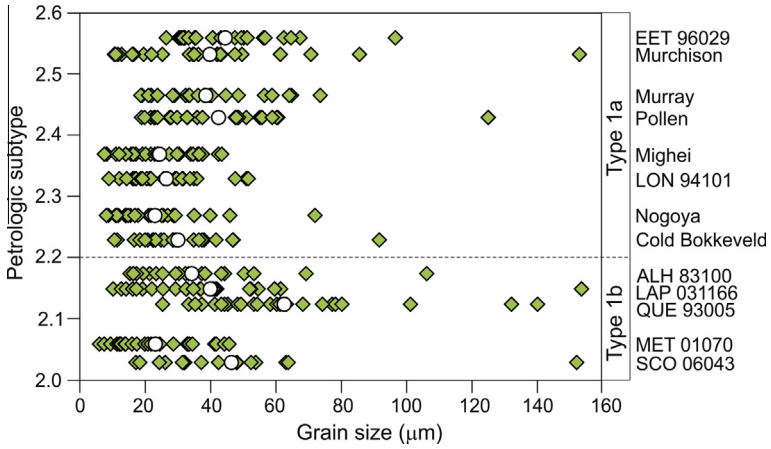

Fig. 4. The sizes of type 1 calcite grains. White circles are the means of each dataset. Grains tend to have a narrower range of sizes in the CM2.3–CM2.2 meteorites, and their average values are also lower. ALH 84005 is not included because it lacks type 1 calcite. $n = 25$ for all meteorites apart for SCO 06043 ($n = 16$).

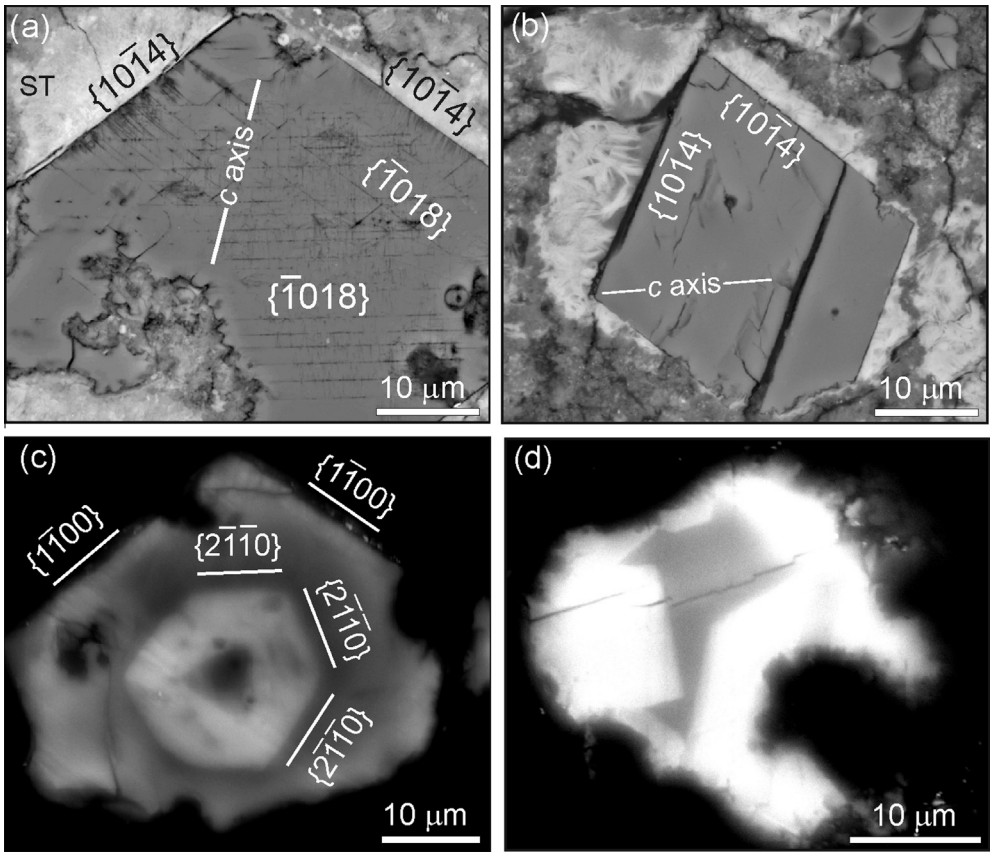

Fig. 5. Crystals of type 1a calcite in meteorite matrices. (a) BSE image of a subhedral crystal in Murray whose two straight edges are in contact with serpentine/tochilinite (ST) whereas its base has an irregular interface with the matrix. Parallel lines are traces of {$\bar{1}$018} *e*-twins, and the straight edges are {10$\bar{1}$4} crystal faces. The *c* axis lies in the plane of the thin section and its orientation is indicated. (b) BSE image of a subhedral crystal in Mighei. Its straight edges are parallel to {10$\bar{1}$4} and are in contact with serpentine/tochilinite (white) whereas its base has an irregular contact with the matrix. The orientation of its *c* axis is indicated. (c) SEM-CL image of a zoned subhedral crystal in Murray. EBSD shows that the *c* axis is inclined at 33° to the plane of the thin section, the boundaries between internal zones are parallel to {2$\bar{1}\bar{1}$0} planes and the sharp upper edges are parallel to {1$\bar{1}$00}. (d) SEM-CL image of an anhedral crystal from Mighei. The pattern of zoning shows that calcite grew inwards from multiple nucleation sites on its edge.

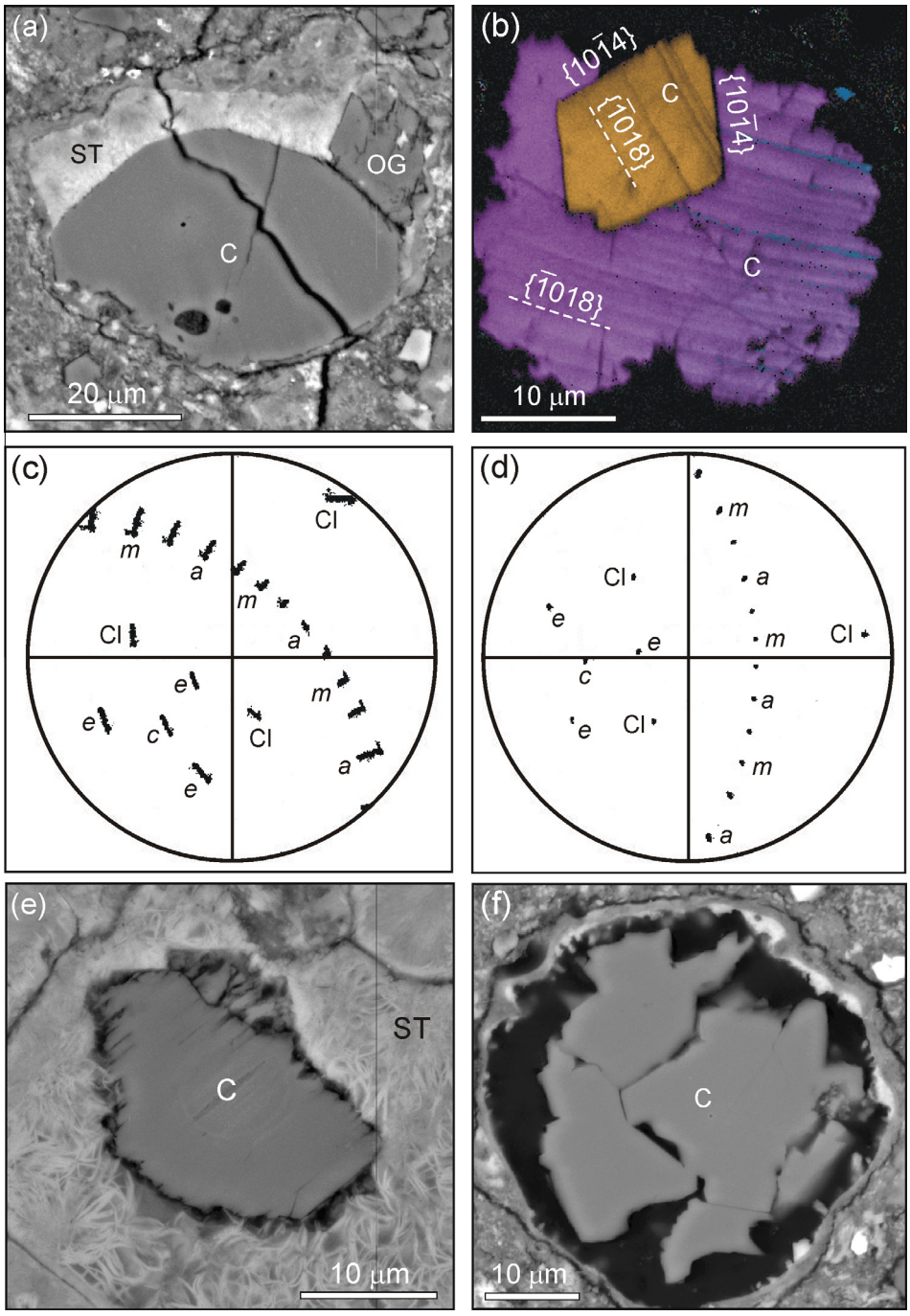

Fig. 6. Type 1a calcite (C) in meteorite matrices. (a) BSE image of a subhedral crystal from Murray that has an irregular base in contact with the matrix, and straight upper edges that are juxtaposed with serpentine/tochilinite (ST). One of the straight edges has a calcite overgrowth (OG). (b) EBSD IPF map (overlain on an IQ map) of a grain in Murray that is composed of two crystals, an initial one that is subhedral and an anhedral overgrowth. The subhedral calcite crystal has a different IPF colour (and so crystallographic orientation) to the overgrowth and a {10$\bar{1}$4} habit. The curving lines in the overgrowth and straight lines in the subhedral crystal are {$\bar{1}$018} *e*-twins. (c) and (d) are EBSD pole figures obtained from the grain in (b) and showing the crystallographic orientations of the overgrowth and subhedral calcite crystal, respectively; *c* is the pole to (0001) (i.e., the *c* axis), *a* is the pole to {2$\bar{1}\bar{1}$0} planes (i.e., the *a* axis), *m* is the pole to {1$\bar{1}$00}, *e* is the pole to the {$\bar{1}$018} *e*-twins, Cl is the pole to the {10$\bar{1}$4} cleavages and the unlabelled points are the poles to {4$\bar{3}\bar{1}$0} planes. The elongation of each cluster of data points in (c) shows that the overgrowth is slightly deformed, which also explains the curvature of its *e*-twins. The subhedral crystal is related to the overgrowth by ~50° anticlockwise rotation about the center of the pole figure. (e) BSE image of a crystal in Cold Bokkeveld that has a wide serpentine/tochilinite rim (ST). Crystal edges are serrated owing to the etching of *e*-twins. (f) BSE image of a grain in Murray whose constituent crystals have been partially etched along their mutual boundaries and around the grain edge. The pore space is occupied by resin (black).

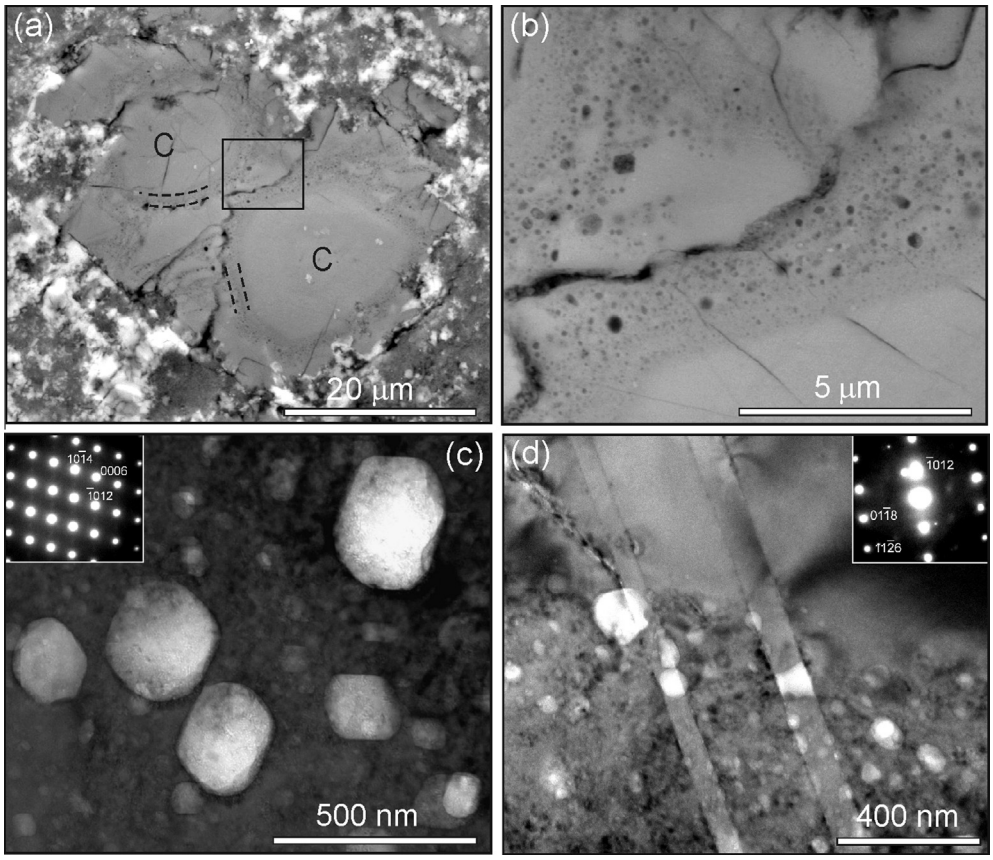

Fig. 7. Nanoporous type 1a calcite (C) in Murchison. (a) BSE image of an equant grain that is comprised of two crystals. Close to the edge of each crystal is a subcircular band of nanopores, and a segment of each band is outlined by parallel dashed black lines. (b) BSE image of the boxed area in (a) showing the 2 bands of nanopores either side of the contact between the two calcite crystals (the irregular line running diagonally across the image). Nanopores increase in diameter from the inside towards the outside of each band. (c) Bright-field TEM image of a foil that was cut from one of the bands of nanopores in (a) and (b). The nanopores are light grey to white, and the inset $[\bar{1}210]$ SAED pattern shows that their shapes are crystallographically controlled and parallel to the traces of $\{10\bar{1}4\}$, $\{0006\}$ and $\{\bar{1}012\}$ planes. (d) Bright-field TEM image of a nanopore-rich area of calcite (lower) that is juxtaposed with a nanopore-free region (upper). Two twins cross between both calcite types, and the inset [4621] SAED pattern shows that they lie parallel to the trace of $\{01\bar{1}8\}$, showing that they are *e*-twins.

systematic differences between types 1a and 1b calcite in their abundance or grain size (Table 4; Fig. 4). Type 1b calcite is uniformly distributed throughout the matrices of 4 of the 5 meteorites in which it occurs. The exception is MET 01070, which contains a centimetre sized sulphide-rich 'lens' (Trigo-Rodríguez and Rubin, 2006; Rubin et al., 2007), and calcite is much less abundant within this lens than in other parts of the sample (Fig. 10).

Type 1b grains have inclusions of coarse euhedral Fe–Ni sulphides, and may also have rims and/or inclusions of phyllosilicates (Fig. 11). For example, calcite grains in ALH 83100 commonly have a ~5 μm wide rim that comprises an outer layer of Fe-rich serpentine and an inner layer of Mg-rich serpentine. By contrast, most type 1b grains in LAP 031166 have a narrow rim of Fe-rich serpentine and also contain fibres of Fe-rich serpentine, typically 10–20 μm long by ~0.5–1.5 μm wide, many of which are encrusted by ~3 μm size Fe–Ni sulphide crystals (Fig. 11a–d). LAP 031166 contains abundant grains that also have a Fe-rich serpentine rim and contain inclusions of Fe-rich serpentine and Fe–Ni sulphide, but Mg-rich phyllosilicate is present in the place of calcite (Fig. 11d). This Mg-rich phyllosilicate has Mg/(Mg + Fe) values of 0.71–0.79 (Supplementary Table 3) and its composition is plotted in Fig. 9. Mg-rich phyllosilicate is also a major constituent of the matrices of ALH 88045, MET 01070 and SCO 06043, where it occurs as tens to hundreds of micrometre size patches in a groundmass of Fe-rich phyllosilicate. The largest of these Mg-rich serpentine patches are oval in shape, suggesting that they are pseudomorphs of flattened chondrules. The compositions of the two phyllosilicate types in both MET 01070 and SCO 06043 are plotted in Fig. 9, and their Mg/(Mg + Fe) values are listed in Supplementary Table 3. The chemical compositions of Mg- and Fe-rich phyllosilicates in the matrix of ALH 88045 were reported by Zolensky et al. (1997) and Lee et al. (2003).

Type 1b calcite grains in LAP 031166 and SCO 06043 commonly have an irregular rim of gypsum, and the sulphate may extend into grain interiors along narrow veins (Fig. 11a and b). The MET 01070 thin section contains numerous irregular pores a few tens of micrometres in diameter, whose size and shape is consistent with an origin by dissolution of type 1b calcite grains.

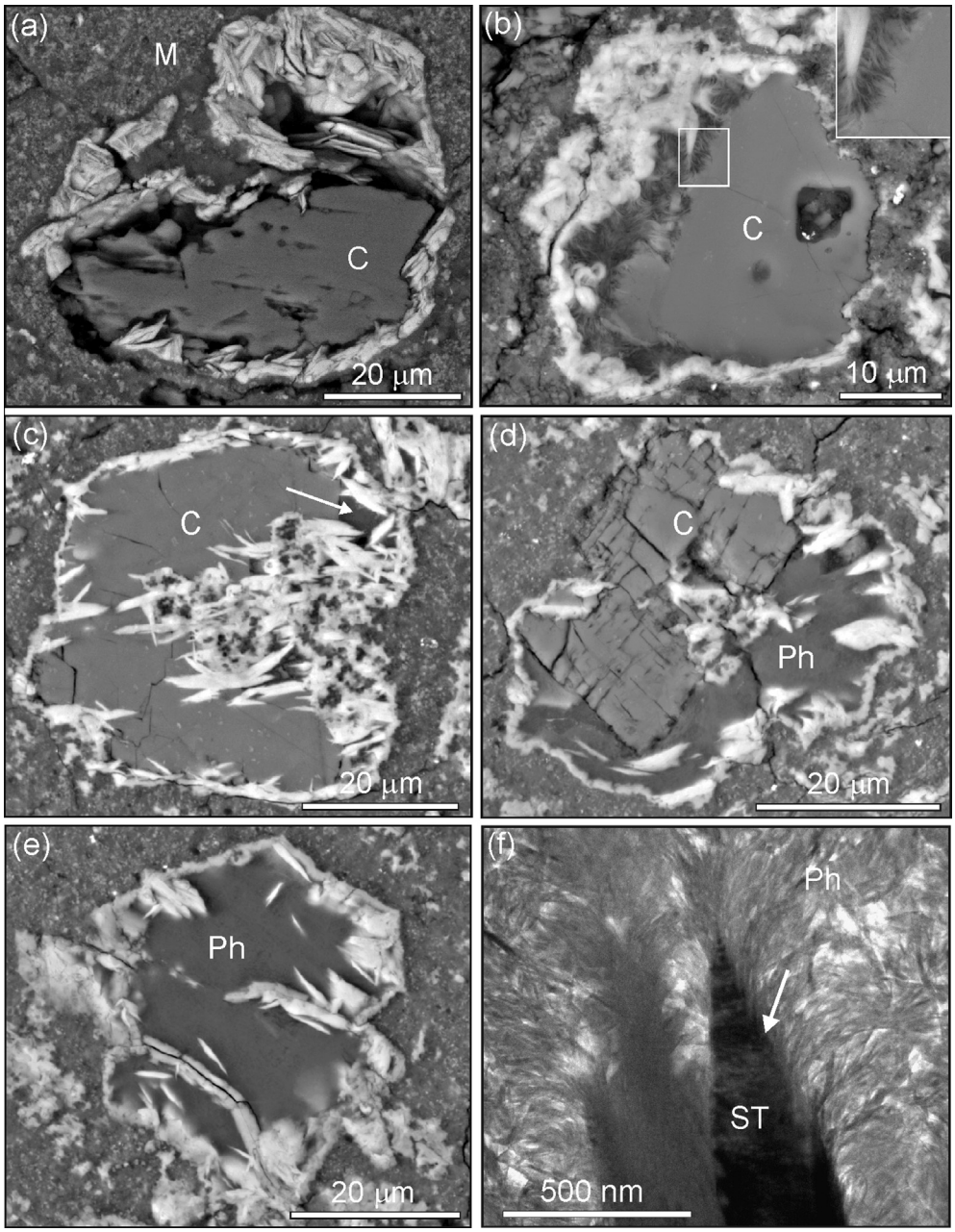

Fig. 8. Crystals of type 1a calcite (C) and associated phyllosilicates (Ph). (a) BSE image of an anhedral crystal in EET 96029 that contains micropores (black) and is rimmed by tabular crystals of a O–S–Fe mineral (white) that penetrate into the calcite. (b) BSE image of an anhedral crystal in Mighei that has a partial serpentine/tochilinite rim (white). The left hand side of the crystal has been replaced by fibres of Mg-rich serpentine, and the inset highlights the penetration of phyllosilicate crystals into the calcite. (c) BSE image of an irregular grain in Pollen that has a continuous serpentine/tochilinite rim, itself encrusted by tochilinite fibres (white). A small patch of Mg-rich serpentine is present in one corner of the grain (arrowed). (d) BSE image of a euhedral grain in Pollen whose serpentine/tochilinite rim is encrusted by tochilinite fibres. Over a third of this grain contains Mg-rich serpentine. (e) BSE image of a Mg-rich serpentine grain in Pollen that is rimmed by serpentine/tochilinite and contains tochilinite fibres (white). (f) Bright-field TEM image of a foil cut from the Mg-rich serpentine intergrown with calcite in Nogoya. The foil predominantly contains finely crystalline Mg-rich serpentine (Ph) but also hosts coarser laths that are composed of an intergrowth of serpentine with tochilinite (ST) and have a characteristic ~1.8 nm basal layer spacing in SAED patterns. These laths are delaminating where in contact with the Mg-rich serpentine (arrowed), and so must have formed earlier.

3.4. Type 2 calcite

Type 2 calcite occurs in 11 of the studied meteorites; 10 host type 2a calcite and only ALH 88045 contains type 2b (Fig. 1). Although type 2 calcite was not observed in the sample of Cold Bokkeveld studied here, chondrule-hosted calcite was described from the same meteorite by Lee (1993), and de Leuw et al. (2010) found that a minority

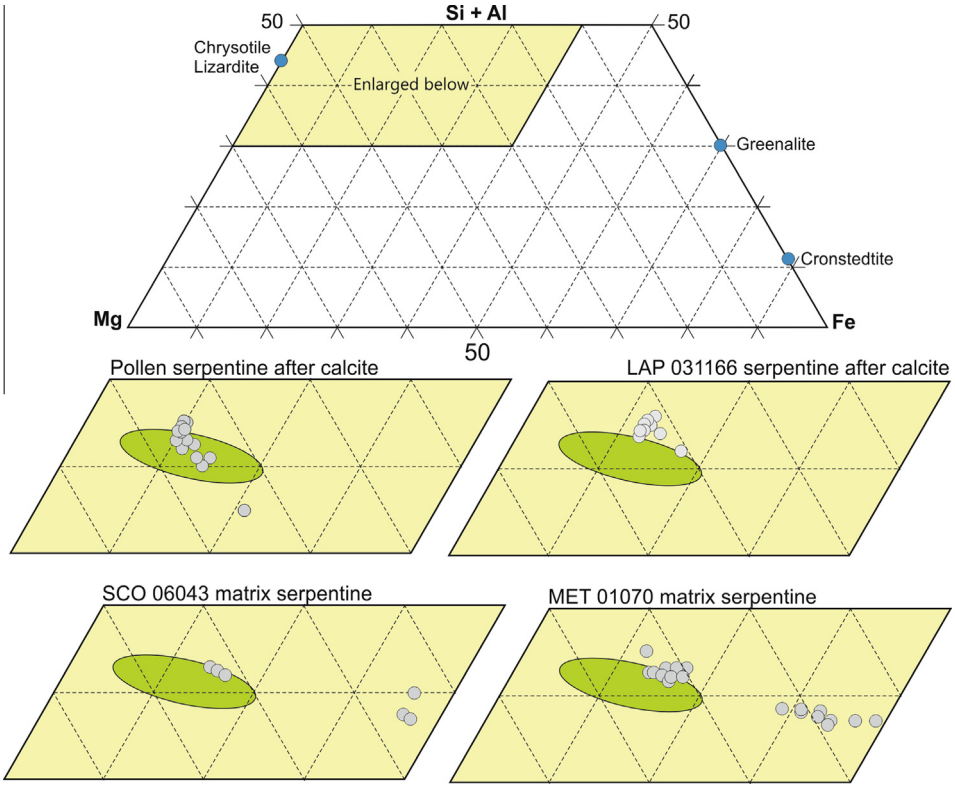

Fig. 9. Ternary diagrams showing the molar element ratios of Mg-rich serpentine grains in Pollen and LAP 031166, and matrix phyllosilicates in SCO 06043 and MET 01070. The compositional range of serpentine after olivine in Nogoya and ALH 81002 is indicated by the oval area (after Velbel et al., 2012).

of calcite grains in Cold Bokkeveld occur as 'aggregates' 40–90 μm in size that have 1–2 μm sulphide inclusions (i.e., consistent with type 2a calcite). Occurrences of type 2 calcite range from rectilinear grains a few tens of micrometers in size to oval/circular objects that can reach 500 μm in diameter (Fig. 12). The oval/circular objects are frequently enclosed by a fine-grained rim analogous to the rims surrounding chondrules (Fig. 12b and c). Type 2a calcite in LON 94101, Mighei and LAP 031166 occurs as patches within otherwise intact chondrules (Fig. 13a). The chondrule-hosted patches in LON 94101 are connected to a millimetre-size calcite vein (Lee et al., 2013a), and all of the LAP 031166 patches have a rim of gypsum (Fig. 13a). Pollen contains a small rectilinear grain of the type 2a calcite that is in contact with a serpentine/tochilinite rimmed grain of Mg-rich serpentine (Fig. 12a). Type 2b calcite is the only carbonate present in ALH 88045, where it comprises 1.1 vol.% of the thin section. The largest type 2b calcite objects are oval in shape, and contain angular patches of phyllosilicate that are comparable in size and shape to areas of mesostasis within porphyritic chondrules (Fig. 13b).

The matrix of Pollen contains a single grain of calcite that is intergrown with enstatite (Fig. 13c). TEM images of a foil that was cut across the calcite-enstatite interface shows that the calcite is free of micropores and inclusions, and its contact with the enstatite is sharp and crystallographically controlled (Fig. 13d). In Mighei calcite occurs in the interior of several calcium- and aluminium-rich inclusions (CAIs).

3.5. Dolomite and breunnerite

In the present study dolomite was found in one CM2.2 (Nogoya), two of the CM2.1 meteorites (ALH 83100 and QUE 93005), and two of the CM2.0s (MET 01070 and SCO 06043) (Fig. 1). It has been described previously from the CMs Cold Bokkeveld (CM2.2), Sutter's Mill (CM2.1-2.0), Y 82042 (CM2–CM2.0), Sayama (CM2.1), EET 83334 (CM2.0) and the paired meteorites ALH 84034/49/51 (CM2.0), Boriskino (CM2.x) and Essebi (CM2.x) (Supplementary Table 1).

3.5.1. Dolomite and breunnerite in the CM2.2 and CM2.1 meteorites

Nogoya contains 2 dolomite crystals, both of which occur in the CM2.3-like lithology along with aragonite and type 1a calcite. These dolomite crystals contain inclusions of phyllosilicate fibres encrusted by euhedral Fe–Ni sulphides, and a rim of coarsely crystalline Mg-rich serpentine that has an interpenetrating contact with the carbonate (Fig. 14a and b). Dolomite is most abundant in the CM2.1 meteorites ALH 83100 and QUE 93005 (Table 4). The ALH 83100 dolomite crystals are anhedral and comparable in size to grains of type 1b calcite in the same meteorite (Table 4). Many of the crystals contain microporous bands

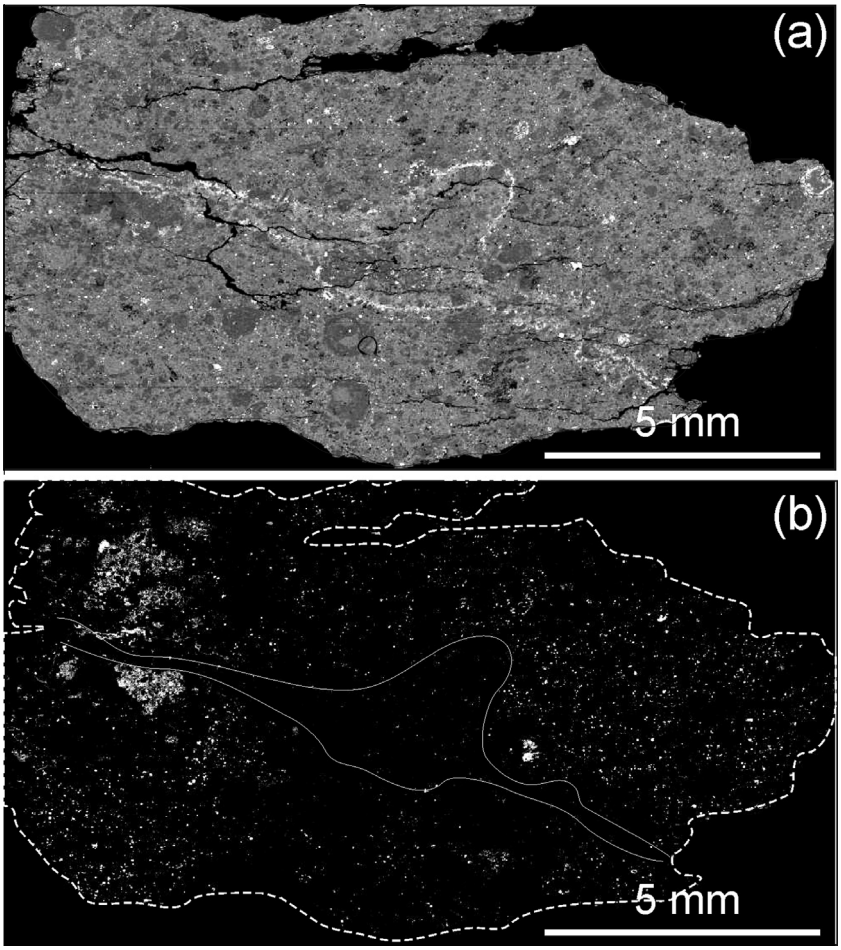

Fig. 10. The MET 01070, 17 thin section. (a) BSE image showing that the thin section is cross-cut by a lens of Fe–Ni sulphide (white band), which extends from the mid-left to lower right, and widens in the centre. (b) Ca K_α X-ray map of the same field of view as (a). The edges of the thin section are outlined by a dashed white line, and the two solid white lines mark the margins of the sulphide lens. Grains of calcite and dolomite (both white) are very rare within the lens. The upper left hand side of the thin section contains several millimetre-sized clusters of calcite and dolomite grains.

or veins of a Mn-rich dolomite, and can also have a large central pore (Fig. 14c). Crystals may have a rim of Fe-rich serpentine, or a multilayered rim with Fe-rich serpentine on the outside and Mg-rich serpentine on the inside (Fig. 14c). QUE 93005 dolomite crystals are anhedral and similar in size to those in ALH 83100 (Table 4). Oscillatory zoning has been recorded by SEM-CL, and all crystals have rims composed of Fe-rich serpentine fibres that are intergrown with subhedral Fe–Ni sulphide crystals (de Leuw et al., 2010; Lee et al., 2012). Dolomite is intergrown with calcite in both QUE 93005 (Lee et al., 2012) and ALH 83100. The ALH 83100 bimineralic grains range from 27 to 149 μm in size (mean 70 μm) and so are on average larger than grains of type 1b calcite and dolomite in the same meteorite (Table 4). Dolomite is usually the dominant carbonate and contains rounded patches of micropore-rich calcite (Fig. 14d).

3.5.2. Dolomite in the CM2.0 meteorites

Dolomite forms less than 1 vol.% of SCO 06043 and MET 01070, but the grains are on average larger than in the other meteorites (Table 4). The SCO 06043 dolomite occurs as individual crystals (Fig. 14e), veins, and bimineralic dolomite-calcite grains (Fig. 14f). The dolomite crystals commonly have inclusions of euhedral Fe–Ni sulphide (Fig. 14e), and may also be rimmed by gypsum. BSE images and Mn K_α X-ray maps reveal that many of them are compositionally zoned, and the zoning pattern indicates crystal growth inwards from grain margins. Most of the larger dolomite grains are dissected by multiple sets of straight and narrow pores that are likely to be etched cleavage planes (Fig. 15a). The SCO 06043 thin section is cross-cut by sub-parallel dolomite veins that are hundreds of micrometres in length. The veins pinch and swell, reaching a maximum of ~10 μm in thickness, and commonly terminate by tapering to a point (Fig. 15b). As the veins are cross-cut by fusion crust they must be pre-terrestrial. This sample also hosts veins of gypsum of a similar size to the dolomite veins, and irregular patches of gypsum that are tens of micrometres in size (Fig. 15a). SCO 06043 dolomite-calcite grains tend to be larger than the dolomite crystals (22–344 μm; mean 100 μm) and often have Fe–Ni sulphide inclusions (Fig. 14f). In most bimineralic grains calcite is the less abundant of the two carbonates, and occurs as

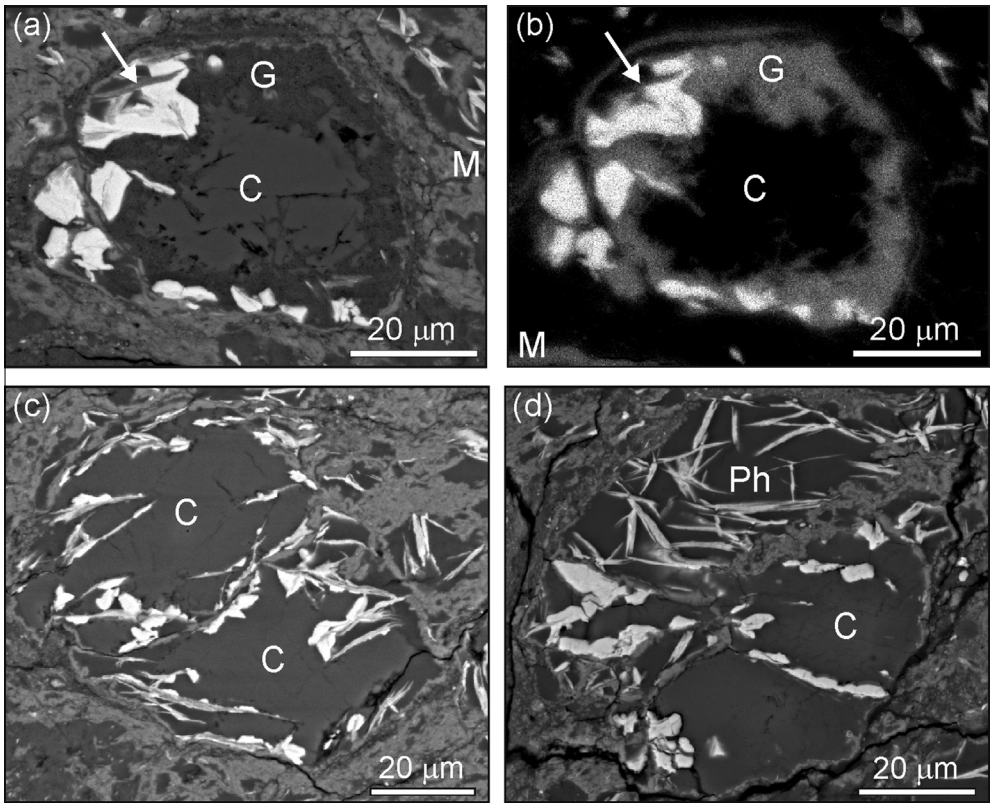

Fig. 11. Images of grains of type 1b calcite (C). (a) BSE image and (b) S K_α X-ray map of an anhedral crystal in LAP 031166. It has a rim of gypsum (G) together with phyllosilicate fibres (arrowed) that are encrusted by crystals of Fe–Ni sulphide (white). (c) BSE image of a grain in LAP 031166. The calcite has inclusions of Fe-rich serpentine fibres, themselves encrusted by Fe–Ni sulphide crystals (white). (d) BSE image of two LAP 031166 grains, both of which have inclusions of phyllosilicate fibres and Fe–Ni sulphides (white). The lower grain contains calcite, whereas the upper grain, which has a very similar mean atomic number, is composed solely of Mg-rich serpentine (Ph).

irregular tens of micrometre size micropore-rich patches within dolomite (Fig. 14f). One of the dolomite-rich bimineralic grains is 344 μm in diameter and oval in shape, suggesting that it is a pseudomorph of a flattened chondrule. MET 01070 dolomite forms large angular patches, most of which are intergrown with type 2a calcite, and are cross-cut by calcite veins (Fig. 16).

3.5.3. Fe-rich carbonates in the CMs

QUE 93005 is the only CM studied that contains breunnerite, which occurs as grains 40–100 μm in size. The breunnerite is also intergrown with dolomite and/or calcite to make bimineralic and polymineralic grains (Lee et al., 2012). Siderite was described by Lindgren et al. (2013) from a millimetre-size clast in LON 94101. The clast contains ~46 vol.% carbonate, which comprises ~10–20 μm size grains of siderite set in a matrix of fine-grained serpentine and saponite.

4. DISCUSSION

4.1. Correspondence between carbonate properties and degree of alteration

Results from the 14 CMs show that the mineralogy, microstructure, and petrographic context of carbonates varies substantially between meteorites, and correlates well with their degree of aqueous alteration. In the discussions below we synthesise these results with information from many of the previous studies of CM carbonates (Supplementary Table 1) to explore: (i) the evolution of aqueous solutions with progressive alteration (i.e., chemical composition, pH, Eh, temperature), and (ii) the origin and interconnectivity of the pore spaces that these fluids occupied, and how porosity and permeability changed with time. It has been assumed that all crystals of each carbonate generation formed synchronously in any one meteorite. However, it remains possible that different minerals precipitated simultaneously in separate parts of a meteorite owing to physical isolation of fluid volumes within the low permeability matrix.

4.2. Early precipitation of carbonates by cementation of pore spaces

4.2.1. Aragonite, breunnerite, calcite and dolomite cements

The aragonite, breunnerite, type 1a calcite and dolomite are interpreted to have grown as cements within fluid-filled pores that were typically a few tens of micrometres in size. A proportion of the type 1b calcite grains are probably also cements, although as discussed later, the presence of corroded crystals of dolomite in type 1b calcite grains from QUE 93005 (Lee et al., 2012) indicates that a proportion

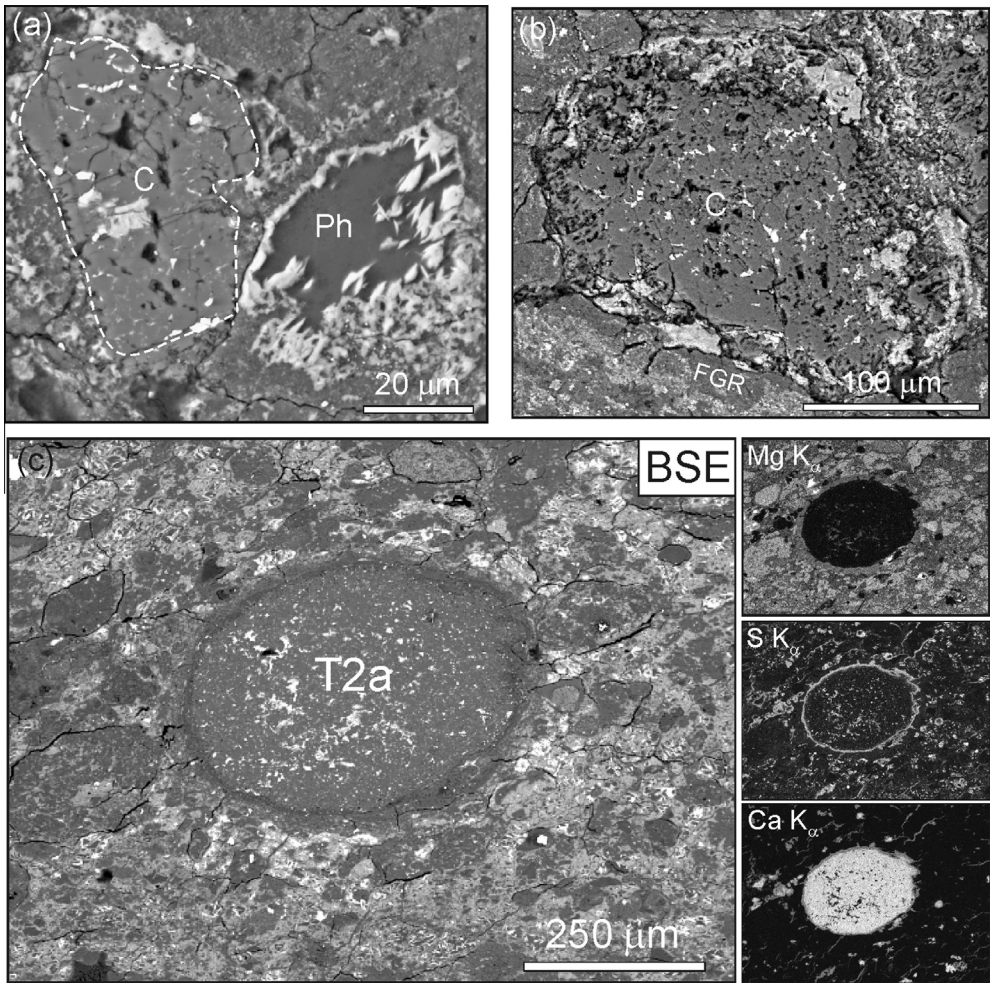

Fig. 12. (a) BSE image of a rectilinear grain of type 2a calcite in Pollen (outlined by a dashed white line) with characteristic inclusions of sulphide (white) and micropores (black). This calcite is in contact with a serpentine/tochilinite rimmed grain of Mg-rich serpentine (Ph). (b) An oval object in EET 96029 that is composed of type 2a calcite, and is enclosed by a fine grained rim (FRG). (c) BSE image and corresponding X-ray element maps of large type 2a object in LAP 031166 (T2a). The object has a narrow fine-grained rim. The Ca K_α and S K_α X-ray maps show that the meteorite matrix is cross-cut by veins of gypsum, and the type 2a object has a continuous rim of gypsum. The Mg K_α map shows that the matrix comprises patches of phyllosilicate of different composition.

of the grains have formed by replacement of dolomite (termed 'dedolomitization'). The evidence for precipitation of the carbonates as cements includes the absence of inclusions of fine-grained matrix, which would be expected if the carbonates had formed within networks of much finer pores in water-saturated regions of the matrix. The subhedral type 1a calcite crystals, which are particularly common in Murchison, Murray and Mighei, also highlight their origin as cements. The faces of these crystals typically abut serpentine/tochilinite, whereas other parts of the crystals are in irregular contact with the matrix (Fig. 5a–c). This common morphology indicates that the subhedral crystals grew from one point on the pore margin (now the irregular crystal edge), but stopped short of completely filling the pore so that crystal faces are preserved. The remaining porosity was later occluded by serpentine/tochilinite. The anhedral crystals and equant/irregular grains of type 1a calcite that occur in all of the CM2.5–CM2.2 meteorites are therefore interpreted to have formed by complete cementation of pore space, and compositional zoning records the former positions of crystal faces (Fig. 5c and d). In the parent body regions sampled by Murchison, Murray and Mighei therefore, crystal growth was unusually slow or short lived so that many of the pores were incompletely filled to leave distinctive subhedral crystals. The oscillatory zoning that is a characteristic of these calcite cements has also been recorded in the present study within crystals of aragonite and dolomite, and zoned dolomite has been previously recorded in QUE 93005 (Lee et al., 2012) and ALH 84049 (Tyra et al., 2010).

Given the very fine grain size of CM matrices, it is unlikely that tens of micrometre size pore spaces could have formed during initial accretion of the parent body and remained open until carbonate precipitation (i.e., it is difficult to envisage how pores that were unsupported from inside could have survived parent body accretion and

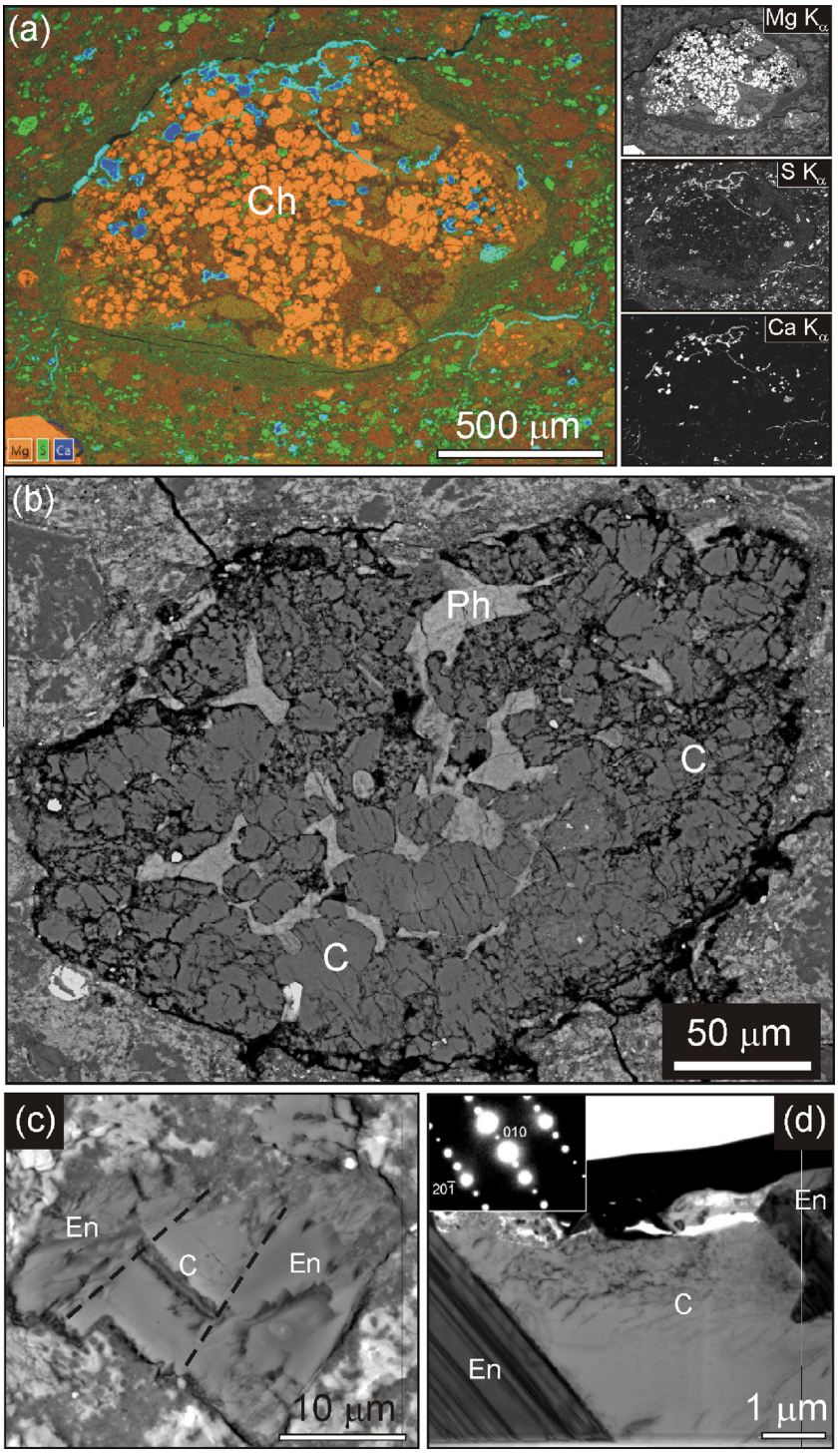

Fig. 13. (a) False coloured multi-element X-ray map and constituent greyscale element maps of a chondrule (Ch) in LAP 031166 that contains patches of type 2a calcite (mainly in its upper part). In the multi-element map the chondrule olivine is orange, calcite is dark blue and gypsum is light blue. All of the calcite patches have a gypsum rim, and veins of gypsum cross-cut the matrix and the chondrule. (b) Oval object in ALH 88045 that contains type 2b calcite. In addition to calcite (C) the object contains patches of Fe-rich serpentine (Ph) whose shape is reminiscent of the mesostasis in porphyritic chondrules. (c) BSE image of an enstatite (En) grain in the matrix of Pollen that is intergrown with calcite (C). The interface between the two minerals is delineated by dashed black lines. (d) Bright-field TEM image of a foil cut across the interface between enstatite (En) and calcite (C) shown in (c). The contact is sharp and planar, and on the left hand side of the image lies parallel to the trace of $(20\bar{1})_{enstatite}$. A [102] SAED pattern of the enstatite is inset. The black band is FIB-deposited platinum. (For interpretation of the references to colour in this figure legend, the reader is referred to the web version of this article.)

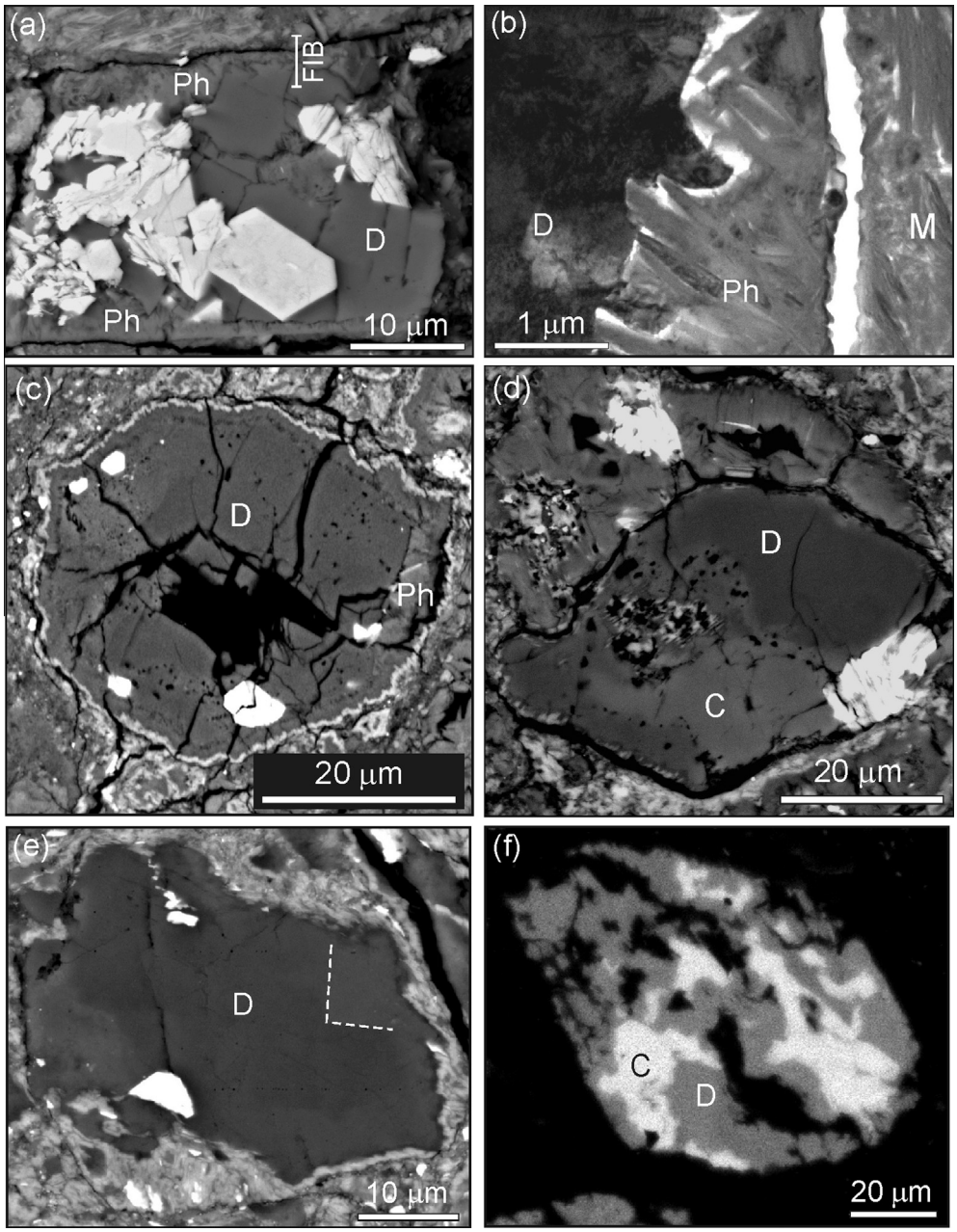

Fig. 14. Images of dolomite (D). (a) BSE image of a crystal in Nogoya that has a narrow phyllosilicate (Ph) rim and contains euhedral Fe–Ni sulphide crystals (white). Most of the Fe–Ni sulphide crystals contain phyllosilicate fibres that are difficult to distinguish from the sulphide owing to their similar mean atomic number. (b) Bright-field TEM image of a foil cut from along the line labelled 'FIB' in (a), which extends from the matrix, through rim phyllosilicates and into dolomite. Crystals within the phyllosilicate rim (Ph) have partially replaced dolomite. These crystals have a ~0.71 nm basal layer spacing, indicative of serpentine, and are rich in both Mg and Fe. The matrix phyllosilicates, to the right of a fracture (white band), are considerably more finely crystalline. (c) BSE image of a dolomite crystal from ALH 83100 that has a central pore (black). The crystal has a narrow outer Fe-rich phyllosilicate rim and an inner rim of Mg-rich phyllosilcate (Ph). It also contains sulphide crystals (white). (d) BSE image of a bimineralic grain in ALH 83100 that contains dolomite intergrown with calcite (C). (e) BSE image of a dolomite grain with sulphide inclusions (white) in SCO 06043. Rectilinear lighter and darker grey areas are compositional zones defined primarily by differences in Mn concentrations. Part of one zone boundary is outlined by the dashed white line. (f) Ca K_α X-ray map of a bimineralic calcite-dolomite grain in SCO 06043 (calcite is white, dolomite grey and matrix is black).

compaction). Instead we suggest that the pores formed by the melting of particles of H_2O-rich ice accompanying internal heating of the parent body.

4.2.2. Implications for the accretion of ice particles

There is little difference in the sizes of type 1 calcite grains between the CMs studied, with few being larger than

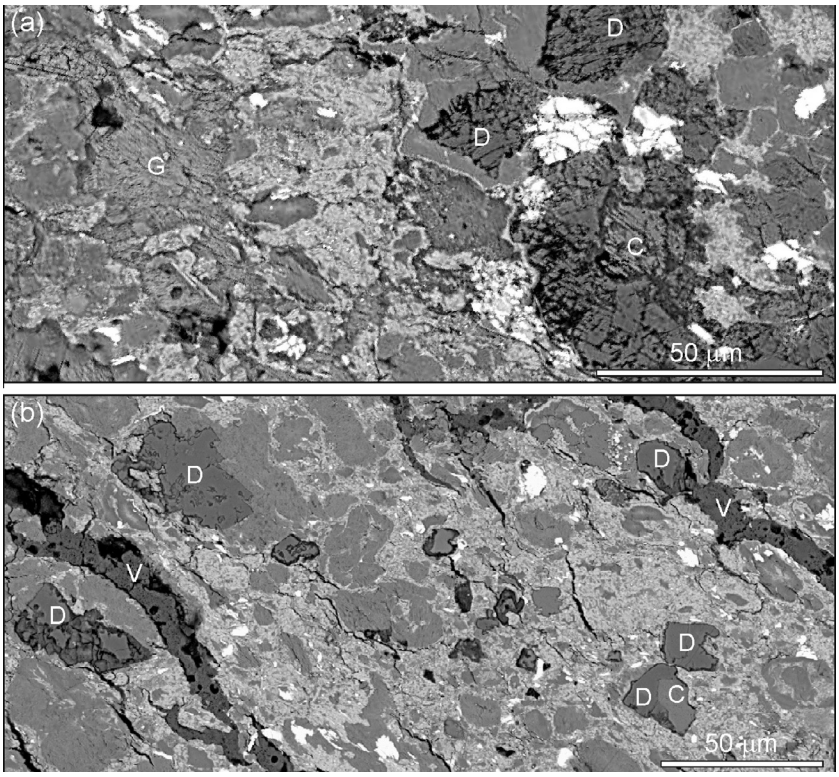

Fig. 15. BSE images of dolomite (D), calcite (G) and gypsum (G) in SCO 06043. (a) An area containing irregular patches of gypsum (left) and dolomite (right). The dolomite has inclusions of sulphides (white) and calcite, and both carbonates have a high density of narrow pores. (b) Two veins (V) of dolomite. The enclosing matrix contains crystals of dolomite and one bimineralic calcite–dolomite grain (lower right).

60 μm, and mean sizes for individual CMs ranging from 22 to 44 μm (Fig. 4) (as described later, the sizes of some CMs carbonate grains have been reduced by partial dissolution and replacement by phyllosilicates). This grain size distribution suggests that the CMs accreted from a reservoir containing ice particles a few tens of micrometres in diameter. The absence of type 1 calcite grains from fine-grained chondrule rims is further evidence for size sorting during parent body formation (i.e., the chondrule rims were formed by accretion of silicate, metal and sulphide grains that were all much smaller than the ice particles). Given the original volumes of ice implied by CM carbonate abundances (i.e., <4 vol.%), not all of the water for aqueous alteration is likely to have come from melting of these particles, and ice is likely to have been present within other parts of the matrix, for example as coatings on primary mineral grains. The likely presence of ice as grain coatings as well as tens of micrometre size particles means that the similarity between meteorites in carbonate abundances does not necessarily indicate that they had the same initial ice/rock ratios.

4.2.3. Carbonate cementation of later fracture pores

The presence of calcite and dolomite veins within some CMs shows that new pore spaces were formed by fracturing after parent body consolidation. A millimetre-size calcite vein occurs in LON 94101 (Lindgren et al., 2011; Lee et al., 2013a), and dolomite veins cross-cut SCO 06043 (Fig. 15b). Veins of dolomite have also been described previously from QUE 93005 (Lee et al., 2012), and ALH 84051 (CM2.0; Tyra et al., 2009). These fractures are most likely to have formed by impact, although there is little petrographic evidence for the timing of opening and cementation of the fractures relative to other parent body processes. Narrow veins containing calcite and dolomite occur in the fine-grained rims to chondrules in QUE 93005 and these fractures were interpreted by Lee et al. (2012) to have formed by expansion of the chondrules during their hydration; very similar veins surround chondrules in the highly altered CM Sutter's Mill (Jenniskens et al., 2012). If the fractures were produced by chondrule expansion, the calcite and dolomite must have formed after significant alteration of the chondrules.

4.3. Solution properties during precipitation of aragonite, calcite and dolomite

4.3.1. Constraints on the continuity of solute supply with progressive alteration

The relationship between the volumes of carbonates in the CMs and their petrologic subtype is a crude indicator of the relative timing of supply of solutes (e.g., Mg, Ca, CO_2). For example, a positive correlation between carbonate volume and petrologic subtype would suggest that solutes were being introduced continuously during alteration, whereas a lack of such a correspondence would imply that once formed, little carbonate was subsequently added (or that late-stage carbonate formed by replacement

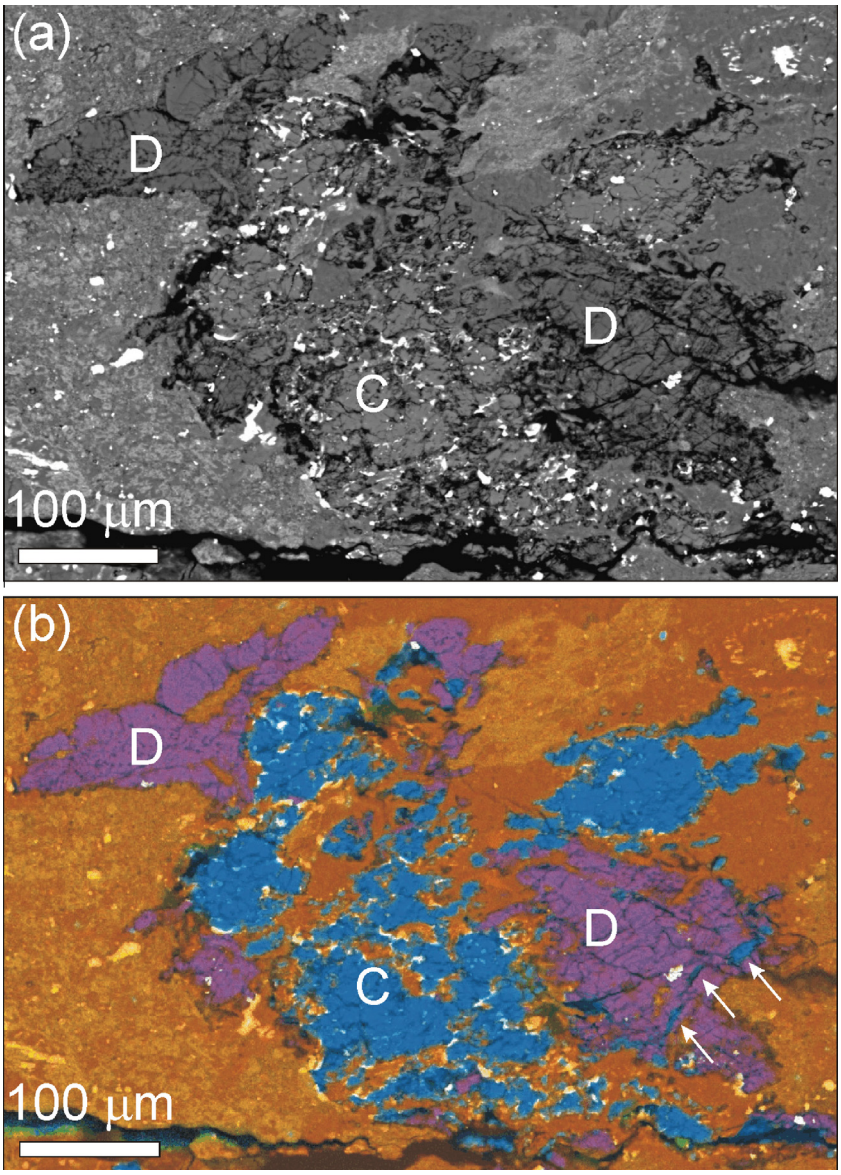

Fig. 16. Dolomite (D) and calcite (C) in MET 01070. (a) BSE image of an intergrowth of dolomite with type 2a calcite. The calcite has inclusions of fine irregular sulphides (white) and micropores (black). The dolomite has a high density of narrow linear micropores, which are absent from the calcite. (b) False coloured multi-element X-ray map of (a) highlighting the distribution of calcite (blue) and dolomite (purple). A vein of calcite cross-cuts dolomite in the lower right hand side of the image (arrowed), and is broken into three segments that are offset by fractures. The enclosing matrix is coloured orange. (For interpretation of the references to colour in this figure legend, the reader is referred to the web version of this article.)

of earlier generations so that there is no net change in carbonate volumes). The abundance of Ca-carbonates in CM meteorites has been previously quantified via the volume of CO_2 liberated upon acid dissolution of bulk samples (Grady et al., 1988; Benedix et al., 2003; Guo and Eiler, 2007; Alexander et al., 2013) (Fig. 17a–c), and none of these studies have found a correspondence with degree of aqueous alteration. Where several splits of the same CM were analysed, the range in carbonate abundance is comparable to the entire range between meteorites. Carbonate volumes (Ca-carbonate plus dolomite) have also been quantified by X-ray mapping of thin sections (Supplementary Table 1), and these data reveal a very weak anticorrelation with petrologic subtype (Fig. 17d). In the present study carbonate abundance was determined by SEM point counting, and data again show little correspondence with degree of alteration, although carbonates are most abundant in two of the CM2.1s (Fig. 17e). These results are consistent with most of the carbonates being formed by cementation of pores after ice particles during early stages of parent body aqueous alteration.

4.3.2. Chemistry of parent body solutions during precipitation of aragonite

Aragonite is assumed to have been the first carbonate mineral to have formed in the CM2.5–CM2.2 meteorites.

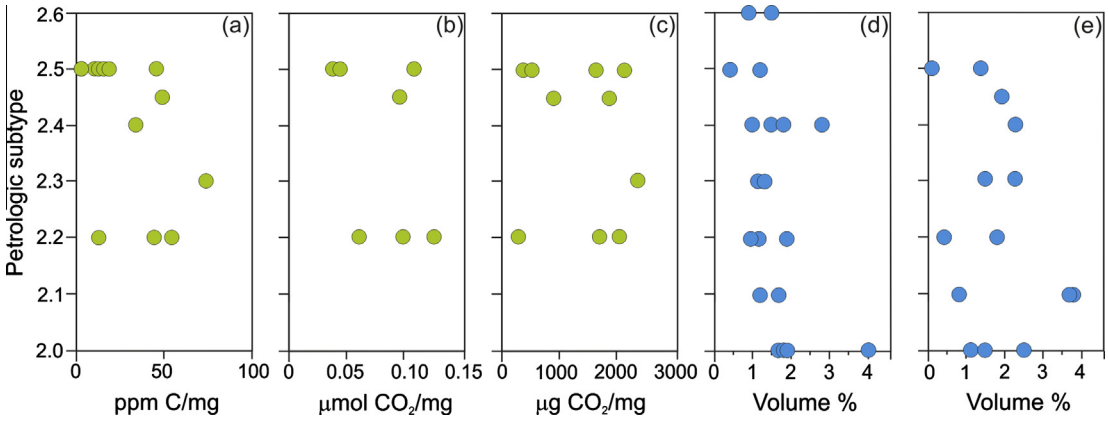

Fig. 17. Plots of carbonate abundance in CMs of different petrologic subtype determined by chemical (a–c) methods and petrographic (d and e) techniques. (a) Grady et al. (1988) treated ~10 to 50 mg samples with 100% phosphoric acid for 18 h at 25 °C, and results for the first extraction are plotted. They analysed 26 CMs, but only data from those CMs with a known petrologic subtype are plotted: Murchison (11 samples), Murray, Pollen, Mighei, Nogoya, Cold Bokkeveld (2 samples). (b) Guo and Eiler (2007) dissolved powdered 40–250 mg samples of 3 CMs in anhydrous phosphoric acid at 25 °C for 18–24 h: Murchison (3 samples), Murray, Cold Bokkeveld (3 samples). (c) Benedix et al. (2003) reacted 360–1050 mg samples of 5 CMs with 100% phosphoric for 18–24 h at 25 °C: Murchison (4 samples), Murray (2 samples), Mighei, Nogoya (3 samples), Cold Bokkeveld. (d) The abundance of carbonates in 13 different CMs determined by previous work: QUE 97990 (Rubin et al., 2007; Howard et al., 2011), Murchison (Brearley et al., 1999; Rubin et al., 2007; Howard et al., 2009, 2011), LAP 04796 (de Leuw et al., 2010), Y 791198 (de Leuw et al., 2010; Howard et al., 2011; Harries and Langenhorst, 2013), Mighei (Howard et al., 2009, 2011), LON 94101 (Lee et al., 2013a), Cold Bokkeveld (de Leuw et al., 2010; Howard et al., 2011), Nogoya (Howard et al., 2009, 2011), ALH 83100 (Howard et al., 2011), QUE 93005 (Howard et al., 2011), LAP 02277 (Rubin et al., 2007), MET 01070 (Rubin et al., 2007; de Leuw et al., 2010; Howard et al., 2011), SCO 06043 (Howard et al., 2011). Values are listed in Supplementary Table 1, and most studies used X-ray mapping. (e) Total carbonate abundance in the 14 meteorites used for the present study, determined by SEM point counting.

The petrographic evidence for this timing comes from Murchison and Pollen where aragonite has been overgrown by type 1a calcite (Fig. 3e). Despite its scarcity in the CMs, aragonite may provide important new information on parent body evolution because it forms under a narrow range of environmental conditions. For example, most abiogenic terrestrial aragonite precipitates from meteoric groundwater or shallow seawater that has a molar Mg/Ca ratio greater than ~1 (Hardie, 1996; Morse et al., 1997). It can form at high pressures in the Earth's mantle (e.g., Humphreys et al., 2010), but such conditions would not have been attained within a CM parent body. Aragonite may also be a good monitor of parent body conditions because in terrestrial rocks it becomes unstable if the chemical composition and/or temperature of ambient aqueous solutions changes appreciably after its crystallization. For example, aragonite precipitated from seawater dissolves readily during diagenesis of sedimentary rocks so that it is essentially absent from pre-Carboniferous deposits. Those Mesozoic and Upper Palaeozoic rocks that have retained aragonite typically have a very low permeability so that grains were physically isolated from diagenetic fluids (e.g., the Buckhorn asphalt; Seuß et al., 2009).

As all CMs that contain aragonite also host calcite, here we explore those factors controlling the polymorph of Ca-carbonate that precipitated from supersaturated parent body solutions. Experiments by Morse et al. (1997) showed that Ca-carbonate polymorphism was controlled principally by the molar Mg/Ca ratio of solutions and temperature. For example, at ~20 °C aragonite precipitates in preference to calcite where molar Mg/Ca is greater than 1, and as temperatures increase to ~40 °C the threshold Mg/Ca ratio falls to ~0.5. The applicability of this empirical model to the CMs can be assessed by determining the Mg/Ca ratios of solutions that were in equilibrium with aragonite and calcite in 6 of the CMs that contain both minerals. These calculations used the chemical compositions of the two minerals together with partition coefficients for Mg into aragonite and calcite (Table 3). The molar Mg/Ca ratios of solutions in equilibrium with aragonite are in excess of 1 for all meteorites apart for Mighei, whereas solutions in equilibrium with calcite are less than 0.3 in all cases (Table 3). These results are consistent with Mg/Ca being the primary control on Ca-carbonate polymorphism in the CMs. Using these estimates of solution Mg/Ca, minimum temperatures during aragonite precipitation can be inferred using the relationships between the two parameters in Morse et al. (1997): Murray and Murchison >13 °C; LON 94101 >19 °C; Cold Bokkeveld and Nogoya >20 °C. For solution Mg/Ca to have controlled the polymorph of Ca-carbonate that formed in Mighei, temperatures would have been greater than ~30 °C. These results are consistent with the temperatures of calcite crystallization derived from clumped isotope thermometry (Murchison 20–33 °C; Murray 30 °C; Cold Bokkeveld 26–71 °C; Guo and Eiler, 2007), with the caveat that these analyses are from bulk samples and so will average intra-meteorite isotopic heterogeneity that has been identified by Tyra et al. (2012), Lee et al. (2013a) and Horstmann et al. (2014). Given that aragonite was the first-formed carbonate in the CM2.5–CM2.2 meteorites, the required Mg and Ca

are likely to have been sourced by dissolution of those primary constituents that were most susceptible to aqueous alteration (i.e., amorphous materials including glass within chondrule mesostases). Both of these components are rarely preserved in the CMs, but amorphous material in the groundmass of the primitive ungrouped carbonaceous chondrite Acfer 094 has a molar Mg/Ca ratio that ranges from 7.0 to 16.2 (Greshake, 1997). Thus, dissolution of amorphous material in CM matrices is likely to have contributed to the high Mg/Ca of early parent body solutions.

The scarcity of aragonite relative to calcite in the CMs could be because much of it was dissolved or replaced, or because the high Mg/Ca solutions were present only briefly and/or in small (i.e., millimetre to sub-millimetre size) parent body regions so that little aragonite precipitated. These possibilities can be evaluated by considering the meteorites in which aragonite occurs. As it has been found in all of the 6 falls studied but only 1 of the 8 Antarctic finds, aragonite could have been lost by terrestrial weathering. However, given that Antarctica is the source of most of the highly aqueously altered meteorites examined in the present study (i.e., all of the CM2.1s and CM2.0s; Table 1), it is more likely that parent body conditions that led to intense aqueous alteration of the CMs were unfavourable to the precipitation or preservation of aragonite. The possibility that aragonite formed in one or more of the CM2.1 and CM2.0 meteorites and was dissolved as aqueous alteration progressed, is supported by the good correlation between the abundance of aragonite crystals in the CM2.5–CM2.2 meteorites, their preservation (as expressed by the proportion of euhedral and subhedral crystals), and the extent of aqueous alteration of their host rock (Fig. 2). Whilst this correlation between aragonite preservation and petrologic subtype is consistent with its complete removal from the CM2.1 and CM2.0 meteorites by dissolution during advanced stages of parent body aqueous alteration, in later sections we also explore the possibility that dolomite formed from the early high Mg/Ca solutions rather than aragonite. Regardless of the explanation for its absence from the highly altered CMs, results of this study show that aragonite is a very sensitive indicator of the availability of liquid water after its precipitation, which in turn is likely to have been a function of the duration of aqueous alteration and/or water/rock ratio. Therefore, the good preservation of aragonite in the CM2.5 and CM2.4 meteorites suggests that aqueous alteration was brief and/or little water was subsequently available, whereas partial dissolution of aragonite in the CM2.3 and CM2.2 meteorites (Fig. 2c) indicates a longer duration of alteration and/or higher water/rock ratios.

The discussions above fail to account for the absence of aragonite from EET 96029. As aragonite is patchily distributed in Murchison, Murray and Pollen, it is possible that EET 96029 has sampled a parent body region between clusters of crystals. A more likely explanation is that aragonite is present, but in common with other CM2s is much less abundant than calcite. As calcite is scarce in EET 96029 (i.e., <0.09 vol.%), the even rarer aragonite crystals would be difficult to locate.

4.3.3. Chemistry of parent body solutions during precipitation of calcite

The estimates of solution chemistry above suggest that transition from precipitation of aragonite to calcite in the CMs was due more to a fall in Mg/Ca than a drop in temperature. Confirmation that temperatures were relatively invariant during Ca-carbonate mineralization comes from oxygen isotope analysis of aragonite and calcite in LON 94101 (Lee et al., 2013a). The difference between oxygen isotopic ratios of these two minerals is consistent with equilibrium isotopic fractionation at the same temperature. As precipitation of aragonite would serve to raise solution Mg/Ca (in a chemically closed system), the significant fall in Mg/Ca prior to precipitation of calcite could have been achieved only if another reaction was removing Mg from parent body solutions at a greater rate than Ca. The most likely reaction is the precipitation of Mg-rich phyllosilicates, which are commonplace in meteorite matrices.

Calcite grains within any one CM have a significant compositional range (e.g., Riciputi et al., 1994; de Leuw et al., 2010, Supplementary Table 2). Riciputi et al. (1994) interpreted this property to reflect fine-scale spatial differences in the chemical composition of carbonate-precipitating solutions due to isolation of fluid volumes by the low permeability matrix (i.e., the chemistry of solutions in individual pores or groups of pores evolved independently). However, the intergranular compositional variability may be due more to trace element zoning of the calcite (Brearley, 2006a), i.e., collection of EMPA data from a suite of chemically zoned crystals will yield a range of compositions unless the analysis points are targeted to specific zones. SEM-CL imaging and elemental mapping has provided good evidence for zoning in type 1 calcite. It is developed most clearly in type 1a grains from the CM2.5–CM2.3 meteorites, specifically Murchison (Brearley et al., 1999; Fujiya et al., 2010; this study), Murray (Lee and Ellen, 2008; this study), Pollen and Mighei (this study), and Y 791198 (CM2.4; Brearley et al., 2001). The polycrystalline grains of type 1a calcite, where an initial subhedral crystal has a later overgrowth (Fig. 6a and b), is additional evidence for multi-stage calcite precipitation. We therefore suggest that the calcite grains in any one CM may have precipitated synchronously and in equilibrium with a common fluid that changed in composition over time (i.e., temporal changes in solution chemistry were of a greater magnitude than spatial differences).

Support for the idea of simultaneous precipitation of calcite grains within and between individual CMs comes from the bands of nanopores that lie parallel to compositional zones in type 1a calcite from Murchison, Murray and Mighei. The crystallographically controlled shapes of some of these nanopores (Fig. 7d) suggests that they are primary fluid inclusions, which have been previously described in the CM carbonates by Saylor et al. (2001). They may have been incorporated during periods of rapid crystal growth, and as the bands of nanopores usually occur close to crystal edges, the nanopore-bearing calcite may have formed during a parent body-wide event, for example depressurisation.

4.3.4. The parent body environment during precipitation of dolomite

As dolomite occurs only in the CM2.2–CM2.0 meteorites, it is potentially important as a recorder of those conditions that led to high degrees of parent body aqueous alteration. On the basis of compositional relationships between CM calcite and dolomite, Riciputi et al. (1994) concluded that the two minerals were not in chemical equilibrium, and that dolomite had formed after calcite. Dolomite must have precipitated prior to the minerals that have replaced it (i.e., Mg- and Fe-rich serpentine and Fe–Ni sulphide). As the same minerals have also replaced type 1 calcite, dolomite must have precipitated at an equivalently early stage in the aqueous alteration history. Such a timing would also be consistent with the findings by Fujiya et al. (2012) of indistinguishable $^{53}Mn/^{53}Cr$ ages for dolomite in ALH 83100 and Sayama, and calcite in Murchison and Y 791198. Lee et al. (2012) concluded that dolomite was the first carbonate mineral to form during aqueous alteration of QUE 93005, and we suggest that dolomite precipitation early in parent body alteration history was the norm.

If type 1a calcite in the CM2.5–CM2.2 meteorites and dolomite in the CM2.1s and CM2.0s both formed as cements soon after melting of H_2O-rich ice particles, the properties of these early-stage solutions must have differed significantly between parent body regions. There has been very little previous discussion of the reasons why dolomite occurs in the CMs, and even in terrestrial rocks the determinants of dolomite precipitation remain poorly understood, as articulated in the 'dolomite problem'. The crux of this problem is that dolomite is very rare in recent terrestrial marine sediments, despite seawater being supersaturated with respect to it, but is commonplace in ancient rocks. Thus the precipitation of dolomite from seawater must be chemically inhibited, and explanations include: (i) hydration of Mg^{2+} ions (meaning that Ca^{2+} enters growing carbonate crystals more easily); (ii) higher activity of HCO_3^- than CO_3^{2-} (incorporation of HCO_3^- into carbonates is hindered by hydrated Mg^{2+} ions); (iii) presence of SO_4^{2-} (Baker and Kastner, 1981; note that the mechanism of sulphate inhibition remains unclear); (iv) fast rates of carbonate crystal growth (which favours the precipitation of aragonite and calcite that have simpler crystal structures than dolomite) (Tucker and Wright, 1990). For dolomite cements to form in the CM carbonaceous chondrites, one or more of these impediments must have been overcome. Terrestrial dolomite cements are favoured in solutions of high pH (so that CO_3^{2-} is present rather than HCO_3^-), and elevated temperatures (so that hydration of Mg^{2+} ions is less of a barrier) (Tucker and Wright, 1990). Thus there may have been a difference in pH and/or temperature between the CM2.5–CM2.2 and the CM2.1–CM2.0 parent body regions. Modelling has shown that solutions rapidly become alkaline during CM aqueous alteration (e.g., Guo and Eiler, 2007) so that pH is unlikely to have differed substantially between source regions of the CM2.5–CM2.2s and CM2.1–CM2.0s. The ubiquitous presence of sulphides intergrown with carbonates also shows that S was in its reduced form so that the presence of SO_4^{2-} was also not a variable. We therefore conclude that the principal reason why dolomite is most abundant in the CM2.1 and CM2.0 meteorites is relatively high alteration temperatures, which agrees with the low $\delta^{18}O$ values of dolomite in Sayama (CM2.1; Nakamura et al., 2003) together with alteration temperatures inferred for the CM2.0 meteorites (Zolensky et al., 1997).

4.4. Parent body conditions accompanying phyllosilicate and sulphide mineralization

The serpentine/tochilinite rims to type 1a grains are interpreted to have formed after calcite precipitation. This relative timing is suggested by the observation that serpentine/tochilinite fills pore spaces that remained in Murchison, Murray and Mighei after the partial occlusion of pores after ice particles by subhedral type 1a calcite crystals. Serpentine/tochilinite has also replaced the edges of type 1a calcite grains, and in LON 94101 this reaction was especially intense so that in some cases all of the calcite has been replaced, to leave serpentine/tochilinite pseudomorphs after the type 1a grains (Lee et al., 2013a). Equations describing this reaction have been provided by Lee et al. (2013a). Type 1b calcite and dolomite have inclusions of Fe–Ni sulphides, sometimes intergrown with Fe-rich serpentine, and the petrographic context of these minerals also indicates that they have formed by replacement of the carbonates. The differences in mineralogy between sulphides replacing type 1a calcite (i.e., tochilinite) and those replacing type 1b calcite and dolomite (i.e., Fe–Ni sulphides) is interpreted to reflects greater alteration temperatures in the CM2.1s and CM2.0s (tochilinite is unstable above 120 °C; Zolensky et al., 1997), although differences in oxygen fugacity between parent body regions may also been an important variable.

Type 1 calcite and dolomite are often intergrown with Mg-rich serpentine, and the relationships between these minerals indicate that the phyllosilicate has replaced the carbonates (e.g., Fig. 14b). The matrices of Pollen, Nogoya, LAP 031166 and SCO 06043 contain patches of Mg-rich serpentine that are of the same size, shape and petrographic context as the type 1 calcite grains; thus, these Mg-rich serpentine patches may have formed by complete replacement of calcite. The replacement reactions may account for the narrower range of calcite grain sizes, and lower mean values, in the CM2.3–CM2.2 meteorites (Fig. 4). The chemical composition of the calcite-associated Mg-rich serpentine varies over a narrow range (Fig. 9). 90% of LAP 031166 analyses have Mg/(Mg + Fe) values of 0.74–0.80, and 96% of Pollen analyses have a Mg/(Mg + Fe) of 0.74–0.84 (Supplementary Table 3). Serpentine that has replaced olivine in the CMs has a comparable composition; Velbel et al. (2012) quoted Mg/(Mg + Fe) values of 0.74–0.80 for ALH 81002 (original data in Hanowski and Brearley, 2001) and 0.80–0.87 for Nogoya. The chemical homogeneity of the ALH 81002 and Nogoya serpentine after olivine is surprising given the much wider compositional range of their precursor silicate grains. Velbel et al. (2012) accounted for this counterintuitive finding by suggesting that the solutions that had mediated serpentinisation were chemically homogenised by diffusion on the meteorite length scale.

Given that essentially all of the cations required for the Mg-rich serpentine that has replaced calcite would need to have been sourced from outside of the carbonate grains, the ambient aqueous system is likely to have had a comparable interconnectivity to the one that serpentinised the olivine and pyroxene; i.e., Mg, Si and Fe were transported by diffusion over meteorite length scales. Indeed it is possible that replacement of calcite grains and chondrule silicates by Mg-rich serpentine was mediated by the same generation of aqueous solutions. As Mg-rich phyllosilicates in the matrices of the CM2.0s MET 01070 and SCO 06043 are compositionally very similar to the Mg-rich phyllosilicate after calcite in Nogoya and Pollen (Fig. 9; Supplementary Table 3), they may also have formed from solutions of a similar bulk chemical composition and homogeneity.

4.5. Late-stage replacive calcite

4.5.1. Replacement of chondrule silicates by type 2 calcite

The oxygen isotope compositions of types 1 and 2 calcite in EET 96006-paired led Tyra et al. (2012) to conclude that type 1 grains had formed first and from solutions that had acquired relatively little of their oxygen by dissolution of parent body silicates. Lee et al. (2013a) obtained very similar oxygen isotope compositions for type 1a and type 2a calcite in LON 94101, and likewise suggested that type 1a calcite was the earlier of the two carbonate generations; this conclusion was also supported by petrographic evidence. Such a relative timing is also consistent with the fact that only the type 1 calcite has been replaced by serpentine/tochilinite, coarse euhedral sulphides and Mg-rich phyllosilicates (i.e., type 2 calcite formed after precipitation of the phyllosilicates and sulphides). The juxtaposition of a rectilinear grain of type 2a calcite with a Mg-rich serpentine pseudomorph after type 1a calcite in Pollen (Fig. 12a) is further evidence that the type 1a grain was replaced by phyllosilicates prior to formation of the type 2a grain.

The presence of patches of type 2a calcite within chondrules indicates that it formed by replacement of silicates, and in many cases replacement has gone to completion to leave objects hundreds of micrometres in size that are composed solely of type 2 calcite. Its microporosity is typical of a replacement product (Putnis, 2002), and the association of type 2a calcite with Fe–Ni sulphides suggests that replacement was mediated by reducing solutions, with the Fe possibly being sourced from the silicates themselves. The replacement of silicate minerals by carbonates, a reaction termed 'carbonation', is commonplace in the Earth's crust (e.g., Matter and Kelemen, 2009) and has also been described from martian meteorites (Tomkinson et al., 2013; Lee et al., 2013b). As discussed by Lee et al. (2013a), the carbonation of CM chondrules is likely to be driven by changes in pH accompanying the reaction of anhydrous silicates with bicarbonate-rich solutions. As it is predominantly a replacement product of olivine and pyroxene, type 2 calcite in the CM2.0 meteorites must have formed before they had reached a level of aqueous alteration equivalent to the ~CM2.2–CM2.1 subtype (i.e., so that some olivine/pyroxene were still present within their chondrules). The CM2.0 meteorites SCO 06043 and MET 01070 both contain oval-shaped objects composed of dolomite that are hundreds of micrometres in size, and so likely to be chondrule pseudomorphs. Following the same reasoning as above, this dolomite must have formed before chondrules in these meteorites had lost all of their original anhydrous silicates (i.e., before they reached the ~CM2.2–CM2.1 subtype). There is no clear correspondence between the abundance of type 2 calcite in the CMs examined for the present study and their degree of aqueous alteration, although a compilation of previous studies (Table 5) suggests a tendency for type 2 calcite to be more common in the highly altered meteorites. This pattern of occurrence suggests that the type 2 calcite formed in a relatively short-lived event fairly late in the history of parent body aqueous alteration.

Formation of type 2 calcite at a relatively late stage raises the question of the origin of the Ca and CO_2, given that most of the primary sources of Ca (e.g., chondrule mesostasis) would have been aqueously altered very early. The most likely late-stage source of Ca is dissolution of aragonite and type 1 calcite, either within the same part of the parent body or another region, and evidence for pre-terrestrial calcite dissolution is found in meteorites including LON 94101 (Lee et al., 2013a) and MET 01070 (Fig. 10b). Tyra et al. (2012) discussed several possible drivers for precipitation of type 2 calcite, and their suggestion of degassing of CO_2 accompanying impact fracturing and concomitant depressurisation is consistent with the finding by Lee et al. (2013a) that the type 2a calcite in one LON 94101 chondrule is continuous with a nearby calcite cemented fracture.

CAIs containing calcite were found in the present study only in Mighei, and they were recorded from the same meteorite by MacPherson and Davis (1994). Calcite-bearing CAIs have been described from four other CMs, and one meteorite has CAIs with dolomite (Table 6). In common with the pattern of occurrence of type 2 calcite, there is little evidence that carbonate-bearing CAIs are any more abundant in the more highly altered CMs, although Greenwood et al. (1994) found that calcite occurs in 8% of Cold Bokkeveld CAIs. Thus in common with chondrules, CAIs may have been replaced by carbonate in a relatively short-lived event.

4.5.2. Replacement of dolomite by calcite

Bimineralic grains made of dolomite intergrown with calcite occur in the CM2.1 and CM2.0 meteorites ALH 83100, QUE 93005, SCO 06043, MET 01070; they have also been described from Sutter's Mill (Jenniskens et al., 2012) and ALH 84049 (Tyra et al., 2010). These grains could have formed either by partial dolomitization of type 1b calcite, or by the incomplete replacement of dolomite by a later generation of calcite (i.e., 'dedolomitization'). The bimineralic grains in ALH 83100, QUE 93005 and SCO 06043 typically comprise micropore-free dolomite that hosts patches of calcite, commonly microporous, and there is usually a curved interface between the two minerals (Fig. 14d and f; Lee et al., 2012). The shape of this interface suggests that one of the carbonates has replaced the other because a planar contact would be expected if the bimineralic grains had

Table 5
CM meteorites with chondrule-hosted calcite.

Meteorite	References
EET 96029 (CM22.5)	This study
Murchison (CM2.5)	This study
Murray (CM2.4/2.5)	Bunch and Chang (1980)
LON 94101 (CM2.3)	Lee et al. (2013a)
Mighei (CM2.3)	This study
EET 96006-paired (CM2.2–CM2.3)	Tyra et al. (2012)
Cold Bokkeveld (CM2.2)	Lee (1993)
Nogoya (CM2.2)	Kerridge and Bunch (1979), Bunch and Chang (1980), Benedix et al. (2003)
ALH 83100 (CM2.1)	Zolensky et al. (1997), de Leuw et al. (2010)
LAP 031166	This study
Y 82042 (CM2–CM2.0)	Zolensky et al. (1997)
ALH 84034 (CM2.0)	Brearley and Hutcheon (2000)
ALH 84049 (CM2.0)	Tyra et al. (2010)
ALH 88045	This study
ALH 81002 (CM2.x)	Brearley (2000, 2006a), Hanowski and Brearley (2001)

The chondrule-hosted calcite described in the present study is in all cases type 2 calcite.

Table 6
CM meteorites with CAI-hosted carbonates.

Meteorite (petrologic subtype)	References
ALH 81002 (CM2.x)	Brearley (2000, 2006a), Hanowski and Brearley (2001)
ALH 81002 (CM2.x)	Brearley (2006a)
Murchison (CM2.5)	Fuchs et al. (1973), Armstrong et al. (1982), MacPherson et al. (1983)
Murray (CM2.4/2.5)	Lee and Greenwood (1994), Guan et al. (2009)
Mighei (CM2.3)	MacPherson and Davis (1994), this study
Cold Bokkeveld (CM2.2)	Lee (1993), Greenwood et al. (1994)
ALH 83100 (CM2.1)	de Leuw et al. (2010)
ALH 84034 (CM2.0)	Brearley and Hutcheon (2000)
ALH 81002 (CM2.x)	Brearley (2000, 2006a), Hanowski and Brearley (2001)

These carbonates are calcite in all instances apart for the CAIs in ALH 81002 that contain dolomite.

formed by a sequential cementation of a pore. It is more likely that the bimineralic grains are products of dedolomitization than dolomitization for two reasons: (i) the presence of micropores in a grain is a signature of an origin by replacement in a wide range of mineral systems (Putnis, 2002), and within the bimineralic grains only calcite is microporous, and (ii) rounded patches of calcite within dolomite crystals are a characteristic of dedolomitization in terrestrial rocks (e.g., Lee and Harwood, 1989; Vandeginste and John, 2012). Dolomite in MET 01070 is cross-cut by a calcite vein, showing that dolomite formed first. This conclusion is also consistent with de Leuw et al. (2010), who proposed dedolomitization as the reason for the lower than expected abundance of dolomite in the CM2.0 meteorites that they had studied. The finding by Lee et al. (2012) that a grain of type 2a calcite in QUE 93005 contained a corroded dolomite crystal suggests that a proportion of the type 2a calcite grains in the CM2.1–CM2.0 meteorites may have formed by complete replacement of earlier dolomite.

The petrographic characteristics of the dedolomite, most notably the microporosity of calcite, can help to constrain the stoichiometry of the replacement reaction. In Eq. (1) one mole of dolomite (64.12 cm^3) is replaced by one mole of calcite (36.93 cm^3):

$$CaMg(CO_3)_2 \leftrightarrow CaCO_3 + Mg^{2+} + CO_3^{2-} \quad (1)$$

This reaction results in substantial volume decrease and creation of 42% porosity, which is much greater than observed. Eq. (2) shows the replacement of one mole of dolomite (64.12 cm^3) by two moles of calcite (73.86 cm^3), which necessitates addition of Ca and results in a 15% volume increase, again counter to observations (after Escorcia et al., 2013):

$$CaMg(CO_3)_2 + Ca^{2+} \leftrightarrow 2CaCO_3 + Mg^{2+} \quad (2)$$

The reaction in Eq. (3) allows for either a small increase or decrease in volume depending on the value of x (after Escorcia et al., 2013):

$$CaMg(CO_3)_2 + (1-x)Ca^{2+} + 2xH^+ \leftrightarrow (2-x)CaCO_3 + Mg^{2+} + xH_2O + xCO_2 \quad (3)$$

A value for x of 0.3 yields a reduction in solid volume of 2.1%, which is consistent with the microporosity of calcite within the bimineralic grains (e.g., Fig. 14d). Eq. (3) shows

that dedolomitization requires an input of Ca^{2+} ions, and the most likely source at this late stage is the dissolution of aragonite and calcite in other parent body regions, for which there is considerable petrographic evidence (see below). Eq. (3) also liberates Mg^{2+}, and as CM dolomite also contains Fe and Mn (not included in the equations above) (Riciputi et al., 1994; de Leuw et al., 2010), all 3 ions would enter solution. The most likely sink of Mg, Fe and Mn is phyllosilicates in the meteorite matrices.

4.6. Congruent carbonate dissolution and gypsum precipitation

Grains of aragonite, type 1 calcite and dolomite in most meteorites examined have evidence for dissolution that has formed pores at grain edges and cross-cutting their interiors (e.g., Fig. 6e and f). The internal pores are often straight and narrow, suggesting that they have exploited planar defects such as *e*-twins and cleavage planes. The etching of calcite in CM falls, for example Murray, Nogoya and Cold Bokkeveld, is likely to have taken place in the parent body environment and as part of the on-going sequence of aqueous alteration reactions; the same generation of solutions may have also been responsible for the dissolution of aragonite. The near-absence of type 1b calcite grains from inside the MET 01070 sulphide lens (Fig. 10b) is also good evidence for pre-terrestrial dissolution (i.e., the solutions from which sulphides precipitated also dissolved calcite). The most heavily etched type 1 calcite grains encountered in this study are in the Antarctic finds (e.g., EET 96029), suggesting that in these cases most dissolution was after the fall of the meteorite. Type 1a and 2a calcite grains in LAP 031166 and SCO 06043 are also commonly rimmed and/or cross-cut by gypsum (Figs. 11a, b and 12c), which is interpreted to have formed by replacement of calcite during Antarctic weathering.

5. A MODEL FOR PARENT BODY AQUEOUS ALTERATION

5.1. Evolution of parent body porosity and permeability

Grains of aragonite, breunnerite, dolomite and type 1a calcite, and a proportion of the type 1b calcite grains, were formed early by cementation of pores produced by the melting of H_2O-rich ice particles. New pore space was formed at intervals by impact, and cementation of these fractures produced calcite and dolomite veins. Owing to the occlusion of pore spaces by the initial carbonate generations, the later pulse of calcite had to make space by replacement of the most soluble and reactive minerals remaining, i.e., dolomite, and anhydrous silicates.

5.2. Evolution of solution chemistry

Carbonates in the CM2.5–CM2.2 meteorites witness four phases of mineralization: (1) aragonite, calcite and dolomite cements; (2) replacive tochilinite ± Fe-rich serpentine; (3) replacive Mg-rich serpentine; (4) replacive calcite. Mg-rich serpentine is more common in the CM2.3–CM2.2 meteorites than CM2.5–CM2.4. The CM2.1 and CM2.0 meteorites have a similar four-phase evolution: (1) dolomite and/or calcite cements; (2) replacive Fe–Ni sulphide; (3) replacive Mg-rich serpentine; (4) replacive calcite (Fig. 18). Below these 4 phases of mineralization are discussed in the context of the 5 stages of CM aqueous alteration that were outlined by Velbel et al. (2012), and in turn draw on an alteration sequence described by Hanowski and Brearley (2001): stage 1, alteration focused on the chondrule mesostasis; stage 2, alteration of fine-grained Fa-rich olivine, metal and sulphide; stages 3 and 4, initial alteration of Mg-rich primary minerals; stage 5, alteration of coarse grained Fo-rich olivine in the more highly processed meteorites (i.e., CM2.2-CM2.0).

5.2.1. Phase 1 – pore-filling carbonates

The Mg, Ca, Mn, Fe and Sr for the aragonite and type 1 calcite are likely to have been derived from dissolution of the most soluble primary components (i.e., Fe-rich silicates, glasses and amorphous materials). Alteration of CAIs, and in particular the leaching of chondrule mesostasis, is believed to have been an important source of Ca (Brearley, 2006b), which is supported by the finding of a chondrule in EET 96029 whose preserved mesostasis glass contains 9–12 wt% CaO (Lindgren and Lee, 2014). Therefore phase 1 of carbonate formation corresponds to stage 1 of Velbel et al. (2012). CO_2 for the carbonates is likely to have come from accreted ices, but could also have been derived from the breakdown of organic matter (Alexander et al., 2013). The clustering of Murchison, Murray and Pollen aragonite crystals in millimetre-size regions suggests that initial solutions in these meteorites were compartmentalised by the low permeability meteorite matrix. Conversely, the homogeneous distribution of aragonite in more highly altered CMs LON 94101 and Mighei indicates a higher initial water/rock ratio.

By the time that type 1 calcite had started to form, the matrix was water-saturated and solution chemistry was diffusionally homogenised, at least on the length scale of an individual meteorite, although trace element zoning shows that fluid compositions fluctuated. The duration of calcite precipitation in Murchison, Murray and Mighei was shorter than in most of the other meteorites so that pores were often incompletely filled to leave distinctive subhedral crystals. The common occurrence of bands of nanopores close to the edges of type 1a calcite crystals in these meteorites may suggest a link between the brief duration of mineralization and fluid inclusion formation; for example, calcite crystals may have grown rapidly owing to depressurisation and concomitant CO_2 degassing. Calcite was the first and only carbonate to form in some of the CM2.1–CM2.0 meteorites, whereas in others dolomite was the initial precipitate. The formation of dolomite in the more highly altered CMs is probably attributable to higher initial temperatures, which also influenced sulphide mineralogy (i.e., tochilinite in the CM2.5–CM2.2s versus Fe–Ni sulphide in the CM2.1–CM2.0 meteorites).

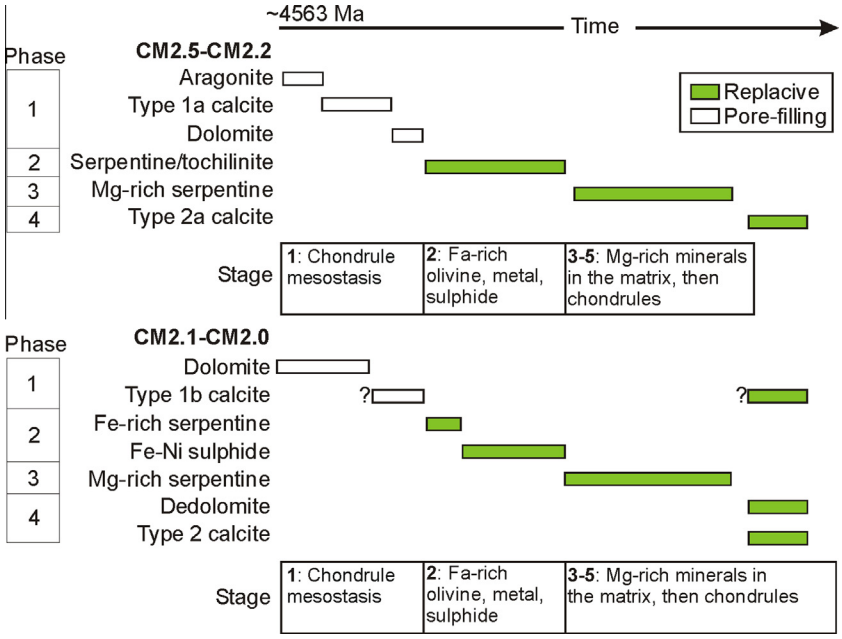

Fig. 18. Summary of the 4 phases of alteration of CM carbonaceous chondrites as defined by carbonates and their intergrown minerals. The CM.5–CM2.2 meteorites have a slightly different mineralization sequence to the CM2.1–CM2.0. These phases are in turn related to the 5 stages of aqueous alteration of the chondrules and matrix as described by Velbel et al. (2012). Precipitation of carbonates started at ~4563 Ma (Fujiya et al., 2012). The alteration of the matrix and chondrules of the CM2.1–CM2.0 meteorites may have lasted longer than for the CM2.5–CM2.2, but the late-stage calcite is shown as forming simultaneously in all parent body regions. ? Indicates uncertainty in the relative timing of type 1b calcite precipitation.

5.2.2. Phase 2 – pore-filling and replacive sulphide and Fe-rich serpentine

In phase 2, Fe-rich serpentine and tochilinite occupied pore spaces remaining in the CM2.5–CM2.2 meteorites (e.g., around the terminations of subhedral calcite crystals), and also replaced the edges of calcite grains to make their serpentine/tochilinite rims. Dolomite and calcite in the CM2.1–CM2.0 meteorites were also replaced by Fe-rich serpentine, commonly as coarse fibres rather than a more finely crystalline rim, and then by Fe–Ni sulphide (rather than tochilinite). The cations required for these replacive minerals would have been sourced by congruent dissolution of highly soluble and reactive matrix minerals (fine-grained metal, sulphide, and Fe-rich matrix silicates), and so phase 2 corresponds to stage 2 of Velbel et al. (2012).

5.2.3. Phase 3 – replacive Mg-rich serpentine

It is long established that the matrices of CM carbonaceous chondrites increase in their Mg/Fe ratio with progressive aqueous alteration (e.g., McSween and Richardson, 1977; McSween, 1979; Zolensky et al., 1993). This change in composition reflects the transition from precipitation of Fe-rich to Mg-rich serpentine, which is in response to the consumption of the most soluble primary Fe-rich minerals (e.g., kamacite; Fa-rich olivine; Fs-rich pyroxene) and initial dissolution of less soluble Mg-rich constituents (e.g., Fo-rich olivine; En-rich pyroxene) (Tomeoka and Buseck, 1985; Zolensky et al., 1993). This process is encapsulated in stages 3–5 of Velbel et al. (2012), and with regards to the present study is expressed by the change in minerals replacing CM carbonates from Fe-rich phases (serpentine, tochilinite, Fe–Ni sulphides) to Mg-rich serpentine. The gap in time represented by the change from Fe-rich to Mg-rich alteration products is difficult to determine, although the distinct difference in chemical composition between the two sets of replacive minerals suggests that there was a considerable hiatus. As replacive Mg-rich serpentine occurs only in the more altered meteorites, it clearly began to form only after the host rock had reached a threshold degree of alteration whereby Mg-rich silicates had started to react.

There is a strong similarity in the chemical composition of the Mg-rich serpentine in three different contexts (Fig. 9): (i) replacing calcite in Pollen and LAP 031166; (ii) in the matrices of MET 01070, SCO 06043, and ALH 88045; (iii) replacing olivine in Nogoya, ALH 81002 and QUE 93005. Velbel et al. (2012) concluded that the intra-meteorite compositional uniformity of Mg-rich serpentine after olivine in Nogoya, ALH 81002 and QUE 93005 reflects diffusional homogenisation of parent body solutions. By extension, the same aqueous system, or at least one with a comparable interconnectivity, is likely to have mediated the replacement of CM carbonates by Mg-rich serpentine.

5.2.4. Phase 4 – replacive calcite

In the final phase of carbonate mineralization, dolomite and remaining anhydrous silicates were replaced by calcite. As this carbonate generation has not been replaced by phyllosilicates or coarsely crystalline sulphides, it must have formed when there was little Mg, Si and Fe entering solution from alteration of primary anhydrous silicates (i.e., towards the end of stage 5 of Velbel et al., 2012). However,

as type 2 calcite in the CM2.0 meteorites replaced chondrules when they still contained some anhydrous silicates, it must have formed before they reached a stage of alteration equivalent to ~CM2.2–CM2.1. The presence of type 2 calcite in meteorites ranging from CM2.5 to CM2.0 further suggests that it does not just form when a threshold degree of host rock alteration has been reached (i.e., its origin is unconnected with the progress of alteration of its host rock). Tyra et al. (2012) suggested that type 2a calcite formed simultaneously in different parent body regions, possibly following impact-induced fracturing and depressurisation. This hypothesis is supported by the presence of type 2a calcite filling a fracture in LON 94101 (Lee et al., 2013a), and the similarity in oxygen isotope compositions of type 2a calcite in LON 94101 and EET 96006-paired (Tyra et al., 2012; Lee et al., 2013a). We therefore speculate that type 2 calcite formed in response to an event that affected many parent body regions simultaneously. Some of these regions had only been altered to CM2.5 level, whereas others had reached CM2.2–CM2.1. In some of these regions aqueous alteration continued after precipitation of type 2 calcite so that remaining anhydrous chondrule silicates were altered to phyllosilicates.

6. CONCLUSIONS

Carbonate minerals in the CM carbonaceous chondrites provide a wealth of new insights into the evolution of parent body porosity and permeability, water/rock ratio and the longevity and chemistry of aqueous solutions. Information pertinent to the use of carbonates and intergrown minerals to track and investigate parent body conditions is as follows:

(1) Crystals of aragonite, breunnerite, calcite and dolomite formed at an early stage of parent body aqueous alteration and by cementation of pore spaces formed by the melting of tens of micrometre-size particles of H_2O-rich ice.
(2) In the CM2.5–CM2.2 meteorites aragonite was the first carbonate to form, and from solutions of a relatively high Mg/Ca ratio and temperatures of more than ~13 °C.
(3) The good preservation of crystals of aragonite in the CM2.5 and CM2.4 meteorites, together with their concentration in clusters, suggests that water/rock ratios were low during their precipitation, and little water was present after they formed.
(4) The abundance of aragonite crystals and their degree of dissolution is a good measure of extent of aqueous processing of their host rock; both properties fall with increasing degree of alteration, reflecting higher water/rock ratios and/or greater longevity of water in the CM2.3–CM2.2 meteorites.
(5) Relatively high initial parent body temperatures, probably in excess of 120 °C, meant that dolomite was the first carbonate to form from the early high Mg/Ca solutions in some of the CM2.1 and CM2.0 meteorites.
(6) The breunnerite, calcite and dolomite cements were replaced by Fe-rich minerals (Fe-rich serpentine; tochilinite; Fe–Ni sulphide), and later by Mg-rich serpentine.
(7) The change over time from Fe-rich to Mg-rich replacement products reflects the evolution of pore fluid chemistry in response to dissolution of Fe-rich then Mg-rich primary minerals.
(8) Intra-meteorite similarities in the chemical composition of the Mg-rich serpentine that has replaced calcite indicates that water/rock ratios were sufficiently high at this relatively advanced stage of aqueous alteration that solution compositions were homogenised on centimetre length scales by diffusion.
(9) The Mg-rich serpentine after calcite may have formed synchronously with Mg-rich serpentine of a very similar chemical composition that has replaced chondrule olivine and pyroxene.
(10) Nearly all CMs contain a second generation of calcite that formed by replacement of the most soluble minerals remaining (i.e., olivine and pyroxene in all CMs, and dolomite in the CM2.1–2.0s). The distinctive oxygen isotope composition of this replacive calcite, and its occasional occurrence in veins, suggests that it may have formed synchronously in different parent body regions, possibly in response to impact fracturing and concomitant depressurisation.

ACKNOWLEDGEMENTS

We are grateful to NASA JSC and the Natural History Museum (London) for loan of meteorite samples used in this study. Peter Chung, William Smith and Colin How are thanked for their assistance with the SEM, FIB and TEM. This research was supported by the UK Science and Technology Facilities Council (STFC) through Grants ST/G001693/1 and ST/K000942/1. We thank Wataru Fujiya and two anonymous referees for comments that have significantly improved the manuscript.

APPENDIX A. SUPPLEMENTARY DATA

Supplementary data associated with this article can be found, in the online version, at http://dx.doi.org/10.1016/j.gca.2014.08.019.

REFERENCES

Alexander C. M. O'. D., Bowden R., Fogel M. L. and Howard K. T. (2013) Carbonate abundances and isotopic compositions in chondrites. *Lunar Planet. Sci.*, 44, #2788 (abstr.)..

Armstrong J. T., Meeker G. P., Huneke J. C. and Wasserburg G. J. (1982) The Blue Angel: I. the mineralogy and petrogenesis of a hibonite inclusion from the Murchison meteorite. *Geochim. Cosmochim. Acta* **46**, 575–595.

Baker P. A. and Kastner M. (1981) Constraints on the formation of sedimentary dolomite. *Science* **213**, 214–216.

Barber D. J. (1981) Matrix phyllosilicates and associated minerals in C2M carbonaceous chondrites. *Geochim. Cosmochim. Acta* **45**, 945–970.

Benedix G. K., Leshin L. A., Farquhar J., Jackson T. and Thiemens M. H. (2003) Carbonates in CM2 chondrites: constraints on alteration conditions from oxygen isotopic compositions and petrographic observations. *Geochim. Cosmochim. Acta* **67**, 1577–1588.

Bland P. A., Jackson M. D., Coker R. F., Cohen B. A., Webber B. W., Lee M. R., Duffy C. M., Chater R. J., Ardakani M. G., McPhail D. S., McComb D. W. and Benedix G. K. (2009) Why aqueous alteration in asteroids was isochemical: high porosity ≠ high permeability. *Earth Planet. Sci. Lett.* **287**, 559–568.

Brearley A. J. (1998) Carbonates in CM carbonaceous chondrites: complex zoning revealed by high resolution cathodoluminescence studies. *Lunar Planet. Sci.* **29**, #1246..

Brearley A. J. (2000) Carbonates in the CM carbonaceous chondrite Allan Hills 81002: occurrences and compositional variations. *Meteorit. Planet. Sci. Suppl.* **35**, A32–A33.

Brearley A. J. (2006a) The action of water. In *Meteorites and the Early Solar System II* (eds. D. S. Lauretta and H. Y. McSween). University of Arizona Press, Tuscon, pp. 584–624.

Brearley A. J. (2006b) The role of microchemical environments in the alteration of CM carbonaceous chondrites. *Lunar Planet. Sci.* **27**, #2074..

Brearley A. J. and Hutcheon I. D. (2000) Carbonates in the CM1 chondrite ALH 84034: mineral chemistry, zoning and Mn–Cr systematics. *Lunar Planet. Sci.*, 31, #1407..

Brearley A. J. and Hutcheon I. D. (2002) Carbonates in the Y791198 CM2 chondrite: zoning and Mn–Cr systematics. *Meteorit. Planet. Sci. Suppl.* **37**, A23.

Brearley A. J., Saxton J. M., Lyon I. C. and Turner G. (1999) Carbonates in the Murchison CM chondrite: CL characteristics and oxygen isotopic compositions. *Lunar Planet. Sci.*, 30, #1301..

Brearley A. J., Hutcheon I. D. and Browning L. (2001) Compositional zoning and Mn–Cr systematics in carbonates from the Y791198 CM2 carbonaceous chondrite. *Lunar Planet. Sci.* **32**, #1458..

Browning L. B., McSween H. Y. and Zolensky M. E. (1996) Correlated alteration effects in CM carbonaceous chondrites. *Geochim. Cosmochim. Acta* **60**, 2621–2633.

Bunch T. E. and Chang S. (1980) Carbonaceous chondrites-II. Carbonaceous chondrite phyllosilicates and light element geochemistry as indicators of parent body processes and surface conditions. *Geochim. Cosmochim. Acta* **44**, 1543–1577.

Ciesla F. J., Lauretta D. S., Cohen B. A. and Hood L. (2003) A nebular origin for chondritic fine-grained phyllosilicates. *Science* **299**, 549–552.

Clayton R. N. and Mayeda T. K. (1999) Oxygen isotope studies of carbonaceous chondrites. *Geochim. Cosmochim. Acta* **63**, 2089–2104.

Connolly, Jr., H. C., Smith C., Benedix G., Folco L., Righter K., Zipfel J., Yamaguchi A. and Chennaouiaoudjehane H. (2007) The Meteoritical Bulletin, No. 92, 2007 September. *Meteorit. Planet. Sci.* **42**, 1647–1694.

de Leuw S., Rubin A. E., Schmidt A. K. and Wasson J. T. (2009) ^{53}Mn–^{53}Cr systematics of carbonates in CM chondrites: implications for the timing and duration of aqueous alteration. *Geochim. Cosmochim. Acta* **73**, 7433–7442.

de Leuw S., Rubin A. E., Schmidt A. K. and Wasson J. T. (2010) Carbonates in CM chondrites: complex formational histories and comparison to carbonates in CI chondrites. *Meteorit. Planet. Sci.* **45**, 513–530.

DuFresne E. R. and Anders E. (1962) On the chemical evolution of the carbonaceous chondrites. *Geochim. Cosmochim. Acta* **26**, 1085–1114.

Escorcia L. C., Gomez-Rivas E., Daniele L. and Corbella M. (2013) Dedolomitization and reservoir quality: insights from reactive transport modelling. *Geofluids* **13**, 221–231.

Fuchs L. H., Olsen E. and Jensen K. J. (1973) Mineralogy, mineral chemistry and composition of the Murchison (C2) meteorite. *Smithson. Contrib. Earth Sci.* **10**, 1–39.

Fujiya W., Sugiura N., Ichimura K., Takahata N. and Sano Y. (2010) Mn–Cr Ages of carbonates in Murchison and ALH 83100 CM chondrites. *Lunar Planet. Sci.* **41**, #1644..

Fujiya W., Sugiura N., Hotta H., Ichimura K. and Sano Y. (2012) Evidence for the late formation of hydrous asteroids from young meteoritic carbonates. *Nat. Commun.* **3**, 627.

Gaetani G. A. and Cohen A. L. (2006) Element partitioning during precipitation of aragonite from seawater: a framework for understanding paleoproxies. *Geochim. Cosmochim. Acta* **70**, 4617–4634.

Grady M. M., Wright I. P., Swart P. K. and Pillinger C. T. (1988) The carbon and oxygen isotopic composition of meteoritic carbonates. *Geochim. Cosmochim. Acta* **52**, 2855–2866.

Greenwood R. C., Lee M. R., Hutchison R. and Barber D. J. (1994) Formation and alteration of CAIs in Cold Bokkeveld (CM2). *Geochim. Cosmochim. Acta* **58**, 1913–1935.

Greshake A. (1997) The primitive matrix components of the unique carbonaceous chondrite Acfer 094: a TEM study. *Geochim. Cosmochim. Acta* **61**, 437–452.

Grossman J. N. (1998) The Meteoritical Bulletin, No. 82, 1998 July. *Meteorit. Planet. Sci. Suppl.* **33**, A221–A239.

Guan Y., Paque J. M., Burnett D. S. and Eiler J. M. (2009) Preliminary nanoSIMS analysis of carbon isotope of carbonates in calcium–aluminium-rich inclusions. *Meteorit. Planet. Sci. Suppl.* **44**, A82.

Guo W. and Eiler J. M. (2007) Temperatures of aqueous alteration and evidence for methane generation on the parent bodies of the CM chondrites. *Geochim. Cosmochim. Acta* **71**, 5565–5575.

Hanowski N. P. and Brearley A. J. (2001) Aqueous alteration of chondrules in the CM carbonaceous chondrite, Allan Hills 81002: implications for parent body alteration. *Geochim. Cosmochim. Acta* **65**, 495–518.

Hardie L. A. (1996) Secular variation in seawater chemistry: an explanation for the coupled secular variation in the mineralogies of marine limestones and potash evaporites over the past 600 m.y. *Geology* **24**, 279–283.

Harries D. and Langenhorst F. (2013) The nanoscale mineralogy of Fe, Ni sulfides in pristine and metamorphosed CM and CM/CI-like chondrites: Tapping a petrogenetic record. *Meteorit. Planet. Sci.* **48**, 879–903.

Horstmann M., Vollmer C., Barth M. I. F., Chaussidon M., Gurenko A. and Bischoff A. (2014) Tracking aqueous alteration of CM chondrites – insights from in situ oxygen isotope measurements of calcite. *Lunar Planet. Sci.* **45**, #1761..

Howard K. T., Benedix G. K., Bland P. A. and Cressey G. (2009) Modal mineralogy of CM2 chondrites by PSD-XRD: Part 1. Total phyllosilicate abundance and the degree of aqueous alteration. *Geochim. Cosmochim. Acta* **73**, 4576–4589.

Howard K. T., Benedix G. K., Bland P. A. and Cressey G. (2011) Modal mineralogy of CM chondrites by X-ray diffraction (PSD-XRD): Part 2. Degree, nature and settings of aqueous alteration. *Geochim. Cosmochim. Acta* **75**, 2735–2751.

Huang Y. and Fairchild I. J. (2001) Partitioning of Sr^{2+} and Mg^{2+} into calcite under karst-analogue experimental conditions. *Geochim. Cosmochim. Acta* **65**, 47–62.

Humphreys E. R., Bailey K., Hawkesworth C. J., Wall F., Najorka J. and Rankin A. H. (2010) Aragonite in olivine from Calatrava, Spain – evidence for mantle carbonatite melts from >100 km depth. *Geology* **38**, 911–914.

Jenniskens P., Fries M. D., Qing-Zhu Y., Zolensky M., Krot A. N., Sanford S. A., Sears D., Bauford R., Ebel D. S., Friedrich J. M., Nagashima K., Wimpenny J., Yamakawa A., Nishiizumi K., Hamajima Y., Caffee M., Weten K. C., Laubenstein M., Davis A., Simon S. B., Heck P. R., Young E. D., Kohl I. E., Thimens M. H., Nunn M. H., Mikouchi T., Hagiya K., Ohsumi K., Cahill T. A., Lawton J. A., Barnes D., Steele A., Rochette P., Verosub K. L., Gattacceca J., Cooper G., Glavin D. P., Burton A. S., Dworkin J. P., Elsila J. E., Pizzerello S., Ogliore R., Schitt-Kopplin P., Harir M., Hertkorn N., Verchovsky S., Grady M., Nagao K., Okazaki R., Takechi H., Hirori T., Smith K., Silber E. A., Brown P. G., Albers J., Klotz D., Hankey M., Matson R., Fries J. A., Walker R. J., Puchtel I., Lee C.-T. A., Erdman M. E., Eppich G. R., Roeske S., Gabelica Z., Lerche M., Nuevo M., Girten B. and Worden S. P. (2012) Radar-enabled recovery of the Sutter's Mill meteorite, a carbonaceous chondrite regolith breccia. *Science* **338**, 1583–1587.

Johnson C. A. and Prinz M. (1993) Carbonate compositions in CM and CI chondrites, and implications for aqueous alteration. *Geochim. Cosmochim. Acta* **57**, 2843–2852.

Kemper F., Jager C., Waters L. B. F. M., Henning T., Molster F. J., Barlow M. J., Lim T. and de Koter A. (2002) Detection of carbonates in dust shells around evolved stars. *Nature* **415**, 295–297.

Kerridge J. F. and Bunch T. E. (1979) Aqueous activity on asteroids: evidence from carbonaceous meteorites. In *Asteroids* (ed. T. Gehrels). University of Arizona Press, Arizona, USA, pp. 745–764.

Lee M. R. (1993) The petrography, mineralogy and origins of calcium sulphate within the Cold Bokkeveld CM carbonaceous chondrite. *Meteoritics* **28**, 53–62.

Lee M. R. and Harwood G. M. (1989) Dolomite calcitisation and cement zonation related to uplift of the Raisby Formation(Zechstein carbonate), northeast England. *Sed. Geol.* **65**, 285–305.

Lee M. R. and Greenwood R. C. (1994) Alteration of calcium- and aluminium-rich inclusions (CAIs) in the Murray (CM2) carbonaceous chondrite. *Meteoritics* **29**, 780–790.

Lee M. R. and Ellen R. (2008) Aragonite in the Murray (CM2) carbonaceous chondrite: implications for parent body compaction and aqueous alteration. *Meteorit. Planet. Sci.* **43**, 1219–1231.

Lee M. R., Bland P. A. and Graham G. (2003) Preparation of TEM samples by focused ion beam (FIB) techniques: applications to the study of clays and phyllosilicates in meteorites. *Mineral. Mag.* **67**, 581–592.

Lee M. R., Martin R. W., Trager-Cowan C. and Edwards P. R. (2005) Imaging of cathodoluminescence zoning in calcite by scanning electron microscopy and hyperspectral mapping. *J. Sediment. Res.* **75**, 313–322.

Lee M. R., Lindgren P., Sofe M., Alexander C. M. O' and Wang J. (2012) Extended chronologies of aqueous alteration in the CM2 carbonaceous chondrites: evidence from carbonates in Queen Alexandra Range 93005. *Geochim. Cosmochim. Acta* **92**, 148–169.

Lee M. R., Sofe M. R., Lindgren P., Starkey N. A. and Franchi I. A. (2013a) The oxygen isotope evolution of parent body aqueous solutions as recorded by multiple carbonate generations in the Lonewolf Nunatak 94101 CM2 carbonaceous chondrite. *Geochim. Cosmochim. Acta* **121**, 452–466.

Lee M. R., Tomkinson T., Mark D. F., Stuart F. M. and Smith C. L. (2013b) Evidence for silicate dissolution on Mars from the Nakhla meteorite. *Meteorit. Planet. Sci.* **48**, 224–240.

Lindgren P. and Lee M. R. (2014) Glassy chondrule mesostasis in EET 96029: a CM3 component of a minimally altered CM2 carbonaceous chondrite. *Meteorit. Planet. Sci. Suppl.* (in press).

Lindgren P., Lee M. R., Sofe M. R. and Burchell M. J. (2011) Microstructure of calcite in the CM2 carbonaceous chondrite LON 94101: implications for deformation history during and/or after aqueous alteration. *Earth Planet. Sci. Lett.* **306**, 289–298.

Lindgren P., Lee M. and Sofe M. (2012) Evidence for multiple fluid pulses in the CM1 carbonaceous chondrite parent body. *Lunar Planet. Sci.* **43**, #1949..

Lindgren P., Lee M. R., Sofe M. R. and Zolensky M. E. (2013) Clasts in the CM2 carbonaceous chondrite Lonewolf Nunataks 94101: evidence for aqueous alteration prior to complex mixing. *Meteorit. Planet. Sci.* **48**, 1074–1090.

Mackinnon I. D. R. and Zolensky M. E. (1984) Proposed structures for poorly characterised phases in C2M carbonaceous chondrite meteorites. *Nature* **309**, 240–242.

MacPherson G. J., Bar Matthews. M., Tanaka T., Olsen E. and Grossman L. (1983) Refractory inclusions in the Murchison meteorite. *Geochim. Cosmochim. Acta* **47**, 823–839.

MacPherson G. J. and Davis A. M. (1994) Refractory inclusions in the prototypical CM chondrite, Mighei. *Geochim. Cosmochim. Acta* **58**, 5599–5625.

Matter J. M. and Kelemen P. B. (2009) Permanent storage of carbon dioxide in geological reservoirs by mineral carbonation. *Nat. Geosci.* **2**, 837841.

McSween H. Y. (1979) Alteration in CM carbonaceous chondrites inferred from modal and chemical variations in matrix. *Geochim. Cosmochim. Acta* **43**, 1761–1770.

McSween H. Y. and Richardson S. M. (1977) The composition of carbonaceous chondrite matrix. *Geochim. Cosmochim. Acta* **41**, 1145–1161.

Metzler K., Bischoff A. and Stoffler D. (1992) Accretionary dust mantles in CM chondrites: evidence for solar nebular processes. *Geochim. Cosmochim. Acta* **56**, 2873–2898.

Morse J. W., Wang Q. and Tsio M. Y. (1997) Influences of temperature and Mg:Ca ratio on $CaCO_3$ precipitates from seawater. *Geology* **25**, 85–87.

Müller W. F., Kurat G. and Kracher A. (1979) Chemical and crystallographic study of cronstedite in the matrix of the Cochabamba (CM2) carbonaceous chondrite. *Tschermaks Min. Pet. Mitt.* **26**, 293–304.

Nakamura T., Nogouchi T. and Yoneda S. (2003) The conditions of aqueous alteration reactions recorded in the Sayama CM2 chondrite. *Meteorit. Planet. Sci. Suppl.* **38**, A47.

Putnis A. (2002) Mineral replacement reactions: from macroscopic observations to microscopic mechanisms. *Mineral. Mag.* **66**, 689–708.

Riciputi L. R., McSween, Jr., H. Y., Johnson C. A. and Prinz M. (1994) Minor and trace element concentrations in carbonates of carbonaceous chondrites, and implications for compositions of co-existing fluids. *Geochim. Cosmochim. Acta* **58**, 1343–1351.

Rubin A. E., Trigo-Rodriguez J. M., Huber H. and Wasson J. T. (2007) Progressive aqueous alteration of CM carbonaceous chondrites. *Geochim. Cosmochim. Acta* **71**, 2361–2382.

Russell S. S., Zipfel J., Folco L., Jones R., Grady M. M., McCoy T. and Grossman J. N. (2003) The Meteoritical Bulletin, No. 87, 2003 July. *Meteorit. Planet. Sci. Suppl.* **38**, A189–A248.

Saylor J., Zolensky M., Bodnar R., Loan L. and Schwandt C. (2001) Fluid inclusions in carbonaceous chondrites. *Lunar Planet. Sci.*, 32, #1875..

Seuß B., Nützel A., Mapes R. H. and Yancey T. E. (2009) Facies and fauna of the Pennsylvanian Buckhorn Asphalt Quarry deposit: a review and new data on an important Palaeozoic fossil Lagerstätte with aragonite preservation. *Facies* **55**, 609–645.

Tomeoka K. and Buseck P. R. (1985) Indicators of aqueous alteration in CM carbonaceous chondrites: microtextures of a

layered mineral containing Fe, S, O, and Ni. *Geochim. Cosmochim. Acta* **49**, 2149–2163.

Tomkinson T., Lee M. R., Mark D. F. and Smith C. L. (2013) Sequestration of Martian CO_2 by mineral carbonation. *Nat. Commun.* **4**, 3662.

Trigo-Rodríguez J. M. and Rubin A. E. (2006) Evidence for parent-body aqueous flow in the MET 01070 CM carbonaceous chondrite. *Lunar Planet. Sci.*, 37, #1104..

Tucker M. E. and Wright V. P. (1990) *Carbonate sedimentology*. Blackwell, Oxford.

Tyra M. A., Farquhar J., Wing B. A., Benedix G. K., Jull A. J. T., Jackson T. and Thiemens M. H. (2007) Terrestrial alteration of carbonate in a suite of Antarctic CM chondrites: evidence from oxygen and carbon isotopes. *Geochim. Cosmochim. Acta* **71**, 782–795.

Tyra M. A., Brearley A. J., Hutcheon I. D., Ramon E., Matzel J. and Weber P. (2009) Carbonate formation timescales vary between CM1 chondrites ALH 84051 and ALH 84034. *Lunar Planet. Sci.*, 40, #2474..

Tyra M. A., Matzel J., Brearley A. J. and Hutcheon I. D. (2010) Variability in carbonate petrography and nanoSIMS $^{53}Mn/^{53}Cr$ systematics in paired CM chondrites ALH 84051, LH 84049, and ALH 84034. *Lunar Planet. Sci.* **41**, #2687..

Tyra M. A., Farquhar J., Guan Y. and Leshin L. A. (2012) An oxygen isotope dichotomy in CM2 chondritic carbonates—a SIMS approach. *Geochim. Cosmochim. Acta* **77**, 383–395.

Vandeginste V. and John C. M. (2012) Influence of climate and dolomite composition on dedolomitization: insights from a multi-proxy study in the central Oman mountains. *J. Sediment. Res.* **82**, 177–195.

Velbel M. A., Tonui E. K. and Zolensky M. E. (2012) Replacement of olivine by serpentine in the carbonaceous chondrite Nogoya (CM2). *Geochim. Cosmochim. Acta* **87**, 117–135.

Velbel M. A., Tonui E. K. and Zolensky M. E. (2013) Compositions of partly altered olivine and replacement serpentine in the CM2 chondrite QUE 93005. *Meteorit. Planet. Sci. Suppl.* **48**, A360.

Weisberg M. K., Smith C., Benedix G., Folco L., Righter K., Zipfel J., Yamaguchi A. and Chennaouiaoudjehane H. (2008) The Meteoritical Bulletin, No. 94, September 2008. *Meteorit. Planet. Sci.* **43**, 1551–1588.

White S. N. (2009) Laser Raman spectroscopy as a technique for identification of seafloor hydrothermal and cold seep minerals. *Chem. Geol.* **259**, 240–252.

Wlotzka F. (1990) The Meteoritical Bulletin. *Meteoritics* **25**, 237–239.

Zolensky M. E., Barrett R. and Browning L. (1993) Mineralogy and composition of matrix and chondrule rims in carbonaceous chondrites. *Geochim. Cosmochim. Acta* **57**, 3123–3148.

Zolensky M. E., Mittlefehldt D. W., Lipschutz M. E., Wang M. S., Clayton R. N., Mayeda T. K., Grady M. M., Pillinger C. and Barber D. (1997) CM chondrites exhibit the complete petrologic range from type 2 to 1. *Geochim. Cosmochim. Acta* **61**, 5099–5115.

Associate editor: Eric Quirico